NASA TN D-118



# TECHNICAL NOTE

## D - 118

# INVESTIGATION OF THE FLOW OVER A SPIKED-NOSE HEMISPHERE-CYLINDER AT A MACH NUMBER OF 6.8

By Davis H. Crawford

Langley Research Center
Langley Field, Va.

NATIONAL AERONAUTICS AND SPACE ADMINISTRATION

WASHINGTON December 1959

NATIONAL AERONAUTICS AND SPACE ADMINISTRATION

TECHNICAL NOTE D-118

# INVESTIGATION OF THE FLOW OVER A SPIKED-NOSE HEMISPHERE-CYLINDER AT A MACH NUMBER OF 6.8

By Davis H. Crawford

## SUMMARY

The shape and nature of the flow over a spiked-nose hemisphere-cylinder was studied in detail at a nominal Mach number of 6.8 and in a Reynolds number range (based on diameter and stream conditions ahead of the model) of $0.12 \times 10^6$ to $1.5 \times 10^6$. Schlieren photographs showed the effect of varying the spike length and Reynolds number upon the shape of the separated boundary and upon the location of transition. The heat transfer and pressure distribution over the body were then correlated with the location of the start of separation, the location of reattachment, and the location of the start of transition.

## INTRODUCTION

Spikes ahead of the blunt noses of bodies of revolution have been considered as a means of drag reduction by a number of investigators in recent years (refs. 1 to 9). In reference 10 gas jets directed into the stream as well as spikes were observed to reduce the drag of a blunt body. One investigation (ref. 11) was reported on the use of spikes along the leading edge of a wing for drag reduction. Heat-transfer tests have shown that the presence of a separated region ahead of a blunt body produced by a spike (ref. 3) will cause a detrimental increase in the heat transfer to a hemisphere nose for a Mach number range of 1.75 to 5.04, and a Reynolds number range of $0.155 \times 10^6$ to $0.83 \times 10^6$ based on the diameter of the model. A recent investigation of spiked-nose bodies at a Mach number of 14 and a Reynolds number of $0.365 \times 10^6$ (ref. 9) has shown the heat transfer to be less than half the blunt-body value. The flow over the separated region and body was believed to be entirely laminar.

A greater heat flux across a turbulent separated boundary than across an attached turbulent boundary has been theoretically predicted

(ref. 12) at a low Mach number but it was pointed out that the ratio of heat flux of the separated boundary to that of the attached boundary is a strong function of Mach number. This ratio was calculated to be 6.3 at a Mach number of 0 for air but was calculated to be only 2.8 at a Mach number of 1.6. More recent experimental results by Larson (ref. 13) are at variance with the theory and have indicated an approximate reduction of 60 percent in the heat transfer under a separated turbulent boundary layer artificially produced with a wire trip just ahead of separation. This disagreement between theory and experiment has been attributed to an incorrect assumption in the theory that the air in the low-velocity, reverse-flow region was drawn into the separated boundary layer at a temperature equal to the wall temperature. For the laminar case the theoretical heat transfer across a separated laminar boundary layer is reduced to about 56 percent of that across an attached laminar boundary layer according to reference 12. Experimental results in this case confirm the theory.

Interest has also been shown in separation phenomena concerned with two-dimensional flow (refs. 14 to 22). Theoretical and experimental results have given an insight into the characteristics of separated regions created by adverse pressure gradients caused either by steps, or by shock boundary-layer interaction. These results show the pressure rise at the start of separation, the shape of the boundary of separation, and the pressure under the separated boundary. These quantities are strongly affected by the Mach number and Reynolds number of the free stream, but are primarily affected by the position of transition and turbulence of the boundary layer with regard to the position of the separated region.

The purpose of this investigation is to present the results of heat-transfer and pressure tests of a spiked-nose hemisphere-cylinder tested at a nominal Mach number of 6.8, and through a Reynolds number range of $0.12 \times 10^6$ to $1.5 \times 10^6$ (based on body diameter) together with a study of the effect of transition position. The range of Reynolds numbers was sufficient to allow study of the separated region on the same model with transition taking place after reattachment, on the separated boundary between separation and reattachment, and ahead of separation. Where possible, the separation phenomena was compared with available theory.

## SYMBOLS

| | |
|---|---|
| $b$ | semihemispherical arc length |
| $C_D$ | drag coefficient |
| $D$ | diameter of cylinder |

| | |
|---|---|
| $F_c$ | nondimensional compressible-flow velocity gradient, $\left(\frac{x_o}{U}\right)\left(\frac{dU}{dx}\right)$ |
| L | length of spike |
| M | Mach number |
| $N_{Nu}$ | Nusselt number |
| p | air pressure |
| q | heat transfer to surface per unit area per unit time |
| Q | total heat transfer to hemisphere nose per unit time |
| r | local radius normal to body axis |
| R | radius of cylinder |
| $R_D$ | Reynolds number based on diameter and free-stream conditions ahead of the model |
| $R_t$ | transition Reynolds number based on local conditions and, for separated flow, upon the distance from the start of separation to the start of transition, or, for attached flow, upon the distance from the start of the boundary layer to the start of transition |
| $R_x$ | Reynolds number based on local conditions and, for separated flow, upon the distance from the start of separation or, for attached flow, upon the distance from the start of the boundary layer |
| s | distance along body generatrix from stagnation point of hemisphere |
| T | temperature |
| U | local velocity at outside edge of boundary layer |
| x | distance along separated boundary from start of separation or along attached boundary from start of boundary layer |
| $x_o$ | distance from front of spike to start of separation |
| $\lambda$ | distance from hemisphere-cylinder juncture to station on cylinder |

$\theta$ conical half-angle of separated boundary at start of separation

$\varphi$ angle from stagnation point on hemisphere

$\tau$ time

Subscripts:

c local conditions on cone of separation

i initial condition at start of run

ns with no spike

t to start of transition

$\infty$ undisturbed free-stream conditions



## APPARATUS

### Tunnel

The present investigation was conducted in the Langley 11-inch hypersonic tunnel described in references 23 and 24. Air is stored at 50 atmospheres pressure and is released through an adjustable pressure regulating valve and an air heater with tube resistance elements of nickel-chromium alloy (replacing the storage heater described in references 23 and 24) to the settling chamber and nozzle. A two-dimensional nozzle constructed of Invar and designed for a Mach number of 7 was used for this investigation. Tunnel calibrations have indicated a Mach number of 6.86 ± 0.04 at a stagnation pressure of 30 atmospheres and at a time of 60 seconds in the central core of uniform flow, which measures about $6\frac{1}{2}$ inches in the vertical direction by about 6 inches in the horizontal direction. The Mach number for these tests, however, had a significant possible variation from 6.86, and this variation is discussed further in a subsequent section.

### Models

Three hemisphere-cylinder models were used in this investigation. These models had been tested previously without spikes and results were reported in reference 25. The interchangeable spikes were installed at the stagnation point where the models had been drilled and tapped to receive them. A cross-sectional view showing construction details of these models is presented in figure 1, and a photograph is shown as figure 2. One of the two larger models was instrumented to provide

heat-transfer data and the other, to provide pressure-distribution data. The smallest model was used only for schlieren photographs which were used in the study of the flow characteristics. All models were constructed of SAE 1020 carbon steel. The dimensions of these models were carefully measured before the parts were assembled with silver solder.

The heat-transfer model was 3.025 inches in diameter, 10.5 inches in length, and varied from 0.098 inch to 0.101 inch in wall thickness. There were 25 thermocouples silver soldered into holes in the model skin so that their effective measuring junctions were located on the inner surface. These thermocouples were of No. 36 gage chromel-alumel wire and were arranged in a spiral of one revolution on the hemisphere and two revolutions on the cylinder. Ten of these thermocouples were located on the hemisphere, fourteen were on the cylinder, and one was on the hemisphere-cylinder juncture as shown in figure 1.

The pressure-distribution model was 3.000 inches in diameter, 10.5 inches in length, and 0.10 inch in wall thickness and contained 16 pressure orifices located as shown in figure 1. Two of the orifices were located on the base of the model. The orifices were 0.040 inch in diameter and were arranged in a spiral of one revolution about the hemisphere in order to reduce any orifice-interference effect. The orifices on the cylinder were also arranged in a spiral of one revolution.

The small model used only for the air-flow study was 1.17 inches in diameter and 5.32 inches in length. The spikes used in this model extended 1.17, 2.34, 3.51, and 4.68 inches from the stagnation point of the hemisphere, and thus were respectively 1, 2, 3, and 4 hemisphere diameters in length. These spikes were constructed from No. 32 drill rod (0.116-in. diam.) and the diameter was very nearly 1/10 the diameter of the hemisphere-cylinder. The spikes used with the large hemisphere-cylinder models extended $1\frac{1}{2}$, 3, 6, 9, and 12 inches from the stagnation point of the hemisphere and were respectively, 1/2, 1, 2, 3, and 4 hemisphere diameters in length. These spikes were machined from 0.300-inch-diameter drill rod and also had a diameter 1/10 that of the hemisphere-cylinder. All spikes were tipped with a nose cone of 10° half-angle.

## Test Conditions

For these tests it was considered important to vary the Reynolds number over the widest possible range. The Reynolds number was controlled primarily through the stagnation pressure, but the incidental variation in stagnation temperature had some effect. The tunnel stagnation pressures used were as low as 3.4 atmospheres and as high as 41.5 atmospheres, and the stagnation temperatures were in the range from about 1040° R to about 1260° R. The tunnel Mach number varies with the tunnel stagnation

pressure from about 6.5 near the start of the low-pressure runs to nearly 6.9 for the high-pressure runs at about 60 seconds after the start. The total range of test Reynolds numbers based on the free-stream conditions ahead of the model and the model diameter was from about $0.12 \times 10^6$ to $1.5 \times 10^6$.

## Instrumentation

The temperature measurements included tunnel stagnation temperature and model skin temperature. The stagnation temperature was measured by shielded thermocouples distributed at various stations in the settling chamber. The potentiometers used for recording these temperatures were 12-channel cyclic printers with a 1-second interval between data points. Skin-temperature thermocouples showing the greatest transient change in temperature were read on instruments with a 1-second full-scale response. Four temperatures were recorded on each instrument, so that each temperature was recorded once every 4 seconds. One skin temperature was read on a pen and ink recording potentiometer to determine the accurate shape of the temperature-time curve.

Model surface pressures were recorded on film by the evacuated capsule instruments described in reference 23. Pressure cells were chosen to give the full-scale deflection as nearly as possible for the measuring station. The stagnation pressure was recorded manually from the indication of a high-accuracy Bourdon gage.

The shape and nature of the flow around the model were obtained from a schlieren system which had a single-pass, vertical Z light path with a horizontal knife edge. This system may be arranged to project the image on a screen for visual observation, or to record the image on still or motion-picture film. The light source for the still photographs was a spark-fired mercury vapor lamp with about 3 microseconds duration. The same lamp was operated continuously with a lower intensity for the motion-picture records. The maximum speed of these records was about 7,000 frames per second.

## TEMPERATURE DATA REDUCTION

A method of evaluating the temperature data to find the rate of heat flow into a hemisphere-cylinder model is outlined in reference 25. In this reference the heat transfer was computed several times during a test by considering not only the time rate change of temperature at each station, but also the net heat storage due to conduction at each station. In the present tests the temperature data were obtained by suddenly subjecting the model to the test flow conditions and by determining the time

rate of change of model temperature near the start of the test. This sudden start was made by bypassing the flow through a secondary circuit until the temperature of the heater mass rose to the working level and then diverting this flow through the test nozzle. The step function of stagnation temperature was not perfect, but the total stagnation temperature was always established within 5 seconds. In order to account for the difference between the actual start and a perfect step-function start, the model temperatures were faired from the values at the time of stagnation-temperature equilibrium to values of the model wall temperature at the start of the test, depending on the trend of the model temperature at times exceeding that for stagnation-temperature equilibrium. An example of this fairing is shown in figure 3. The scale increments used in the fairing have been exaggerated for clarity.

Several advantages are inherent in this quasi-step start method of heat-transfer evaluation. The isothermal temperature distribution at the start of the test circumvents the need for heat-conduction corrections, and the radiation from the model near the start of the test is negligible. This constant skin temperature allows available isothermal heat-transfer theories to be applied more correctly. Furthermore, at the start of the test the temperature differential across the boundary layer is higher than at times later in the run, and a small uncertainty in the evaluation of the adiabatic wall temperature will cause a smaller error in the evaluation of the film coefficient of heat transfer near the start of the test.

As a means of establishing the accuracy of this quasi-step start method of securing heat-transfer results, the model was tested in this manner without a spike, and these results were compared with results given in reference 25 which represent a careful attempt to measure heat transfer to this same model at several different wall temperatures while accounting for conduction within the model and radiation losses. The present results scattered around the original data from reference 25 with an average deviation of 12 percent. In the light of the inherent inaccuracies of experimental aerodynamic heating measurements, this agreement was regarded as satisfactory.

The uncertainty associated with experimental recovery temperature measurements is avoided by presenting the results in terms of the ratio of the local heat-transfer rate with a spike to the heat-transfer rate at the stagnation point of the hemisphere without a spike. The value of the heat transfer at the stagnation point of the hemisphere was calculated for each set of tunnel conditions from the experimentally determined value of the nondimensional heat-transfer coefficient determined in reference 25.

## RESULTS AND DISCUSSION

### Flow Characteristics

Nature of the flow about the separated boundary.- Observations of the shape and nature of the flow over this body show trends similar to the findings for similar body shapes in references 1 to 9 and show general separated flow trends obtained on dissimilar bodies in references 14 to 22. Flow separated from the surface of the spike ahead of the blunt body because the pressure rise of the hemisphere nose exceeded the maximum allowable for attached laminar boundary-layer flow. The flow boundary of the hemisphere-cylinder was then effectively transformed to a flow boundary more nearly like that of a cone-cylinder.

A qualitative idea of the effect of the different spike lengths and different test Reynolds numbers upon the flow is shown in the schlieren photographs of figure 4. The flow separated from the tip of the cone forming the nose of the spike with $L/D = 1/2$, but separated close to the cone-cylinder juncture of the spike with $L/D = 1$. The start of separation was apparently fixed at the cone-cylinder juncture of spike with $L/D = 2$ but always occurred behind the cone-cylinder juncture for spikes with $L/D = 3$ and 4. Thus, the start of separation first moved forward with the nose of the spike as the spike increased in length until the start of separation was no longer fixed to the cone-cylinder juncture with a further increase in the spike length. Consequently, the start of separation remained a nearly constant distance ahead of the blunt nose until transition occurred near the start of separation, at which time the start of separation moved back toward the blunt nose.

It has been shown experimentally and theoretically (refs. 16 and 18) that the extent of separation over a two-dimensional separated region is a strong function of the Reynolds number when transition starts anywhere on the separated boundary and that the extent of the separated region of such a transitional boundary layer is reduced by an increase in Reynolds number. The start of transition on the separated boundary can be detected from the flow photographs (fig. 4) by the disappearance of the white line of the laminar separated boundary, or by the appearance of a speckled region in the background of the separated flow. The schlieren photographs of the separated flow over the spikes at the lowest stream Reynolds numbers show little or no evidence of unsteady flow on the separated boundary. As the Reynolds number increases, the start of transition can be seen moving forward on the boundary of separation, and there is evidence of some waves of unsteady flow of small amplitude and high frequency, but the shape of the separated region shows little change. The start of separation from the spikes having values of $L/D$ of $1/2$, 1, and 2 apparently moves forward slightly with a further increase in Reynolds number, even after the start of transition is located on the separated boundary.

The movement of the start of separation on the spikes with $L/D = 3$ and 4 is greater than that for the shorter spikes and is shown in figure 5. The data for the spike with $L/D = 3$ follow the trend of the laminar theory of reference 18, even though transition exists on the separated boundary over much of the Reynolds number range. The data for a spike with $L/D = 4$ show the forward movement predicted by the laminar theory and then the rearward movement characteristic of the turbulent theory. This rearward movement did not occur until transition had moved to the region of the start of separation. The theory of reference 18 is not expected to follow the data for a spike length of 4 diameters accurately, however, since a constant pressure coefficient was assumed at the start of separation when this trend was evaluated. There were slight changes in the extent of separation during a test. These changes were random, or could be explained by a change in flow conditions during a test. The varying temperature of the model had little effect on the extent of separation, as had been found in tests at lower Mach numbers (refs. 20 and 21).

L
2
4
8

The effect of Reynolds number and spike length on the conical half-angle of separation of the laminar boundary layers is shown in figure 6. As the spike length is increased, the angle of separation of the laminar boundary-layer is reduced. The angle of separation from the spike has been computed for both a conical shock and for an oblique shock from the ratio of the local stream Mach numbers after and before separation as determined in reference 14 for the two-dimensional case. For this calculation it was assumed that $M = 6.8$ and $F_c = 0$, where $F_c$ is the nondimensional compressible velocity gradient $(x_o/U)(dU/dx)$ at the start of separation. The calculations for the conical shock are seen to agree roughly with much of the data for spike lengths of 3 and 4 diameters. The calculations for the other spikes do not agree since the forward movement of the start of separation was limited by the nose of the spike.

It is apparent that the angle of separation is a weak function of Reynolds number for all tests except those with spike lengths of 4 diameters at Reynolds numbers (based on diameter) above about $0.8 \times 10^6$. Furthermore, at least part of the small decrease observed in the angle of separation as compared with that of the shorter spikes for the Reynolds number increase from $0.12 \times 10^6$ to $0.7 \times 10^6$ is ascribed to the accompanying Mach number increase from approximately 6.5 to 6.8. The data for the spike length of 4 diameters show a decrease in the separation angle as the Reynolds number increases to about $0.8 \times 10^6$, but as transition begins to occur ahead of separation, the separation angle increases with a further increase in Reynolds number. The flow over the spike at the start of separation for the tests does not appear to be fully turbulent, however, since the data has not reached a level where it is unaffected by a change in Reynolds number as is expected for the fully turbulent case (refs. 14 and 15).

Transition was not observed anywhere on the model when tested without a spike in the Reynolds number range (based on free-stream conditions and body length) of $0.49 \times 10^6$ to $3.69 \times 10^6$. The range of Reynolds numbers to transition for flow along a relatively sharp-leading-edge hollow cylinder in the 11-inch hypersonic tunnel have been shown (ref. 26) to be approximately $1 \times 10^6$ to $5 \times 10^6$ for a stream Reynolds number range of from $0.15 \times 10^6$ per inch to $0.45 \times 10^6$ per inch. The start of transition for the spiked-nose body was observed on the separated boundary or ahead of it for all tests at Reynolds numbers based on stream conditions and the hemisphere-cylinder length above about $0.5 \times 10^6$. The lowest Reynolds number based on the length of the boundary layer to transition occurred as a result of a test of the spike with $L/D = 1/2$ and was about $0.06 \times 10^6$ based on the stream conditions ahead of the model and the boundary length to transition. Thus, it is seen that much lower transition Reynolds numbers were realized on the spiked-nose body. This result suggests the use of spikes or of other separation-producing devices to trip the boundary layer when early transition is desired.

L
2
4
8

Transition Reynolds numbers on the separated boundaries.- The transition Reynolds numbers for the separated boundary layer have been evaluated and correlated on the basis of the distance from the start of separation to the start of transition, as suggested in reference 16. These distances to transition for the various spikes as a function of free-stream Reynolds number based on diameter are shown in figure 7. At the lowest values of $R_D$ for spike lengths of 3 and 4 diameters, the flow on the separated boundary appeared to be entirely laminar. These cases have been plotted in figure 7, where the total length of the separated region is used as the characteristic length, with arrows to indicate that possible transition lengths are greater than the plotted values. For a Reynolds number above about $0.8 \times 10^6$ there is no evidence of laminar flow over the separated region on the spike with $L/D = 4$, and with increasing Reynolds number above this approximate value, transition moves out ahead of the separated region. The stream conditions used in the transition Reynolds numbers are the local flow conditions for a cone of the same angle as the cone of separation of the laminar boundary shown in figure 6. The local pressures and the local Mach numbers for these cone angles are shown in figures 8 and 9, respectively. The pressure over the separated region has been computed for both a conical shock and for an oblique shock from the ratio of the local stream Mach numbers after and before separation as determined in reference 14 for the two-dimensional case. For this calculation it was assumed that $M = 6.8$ and $F_c = 0$ as was done previously in the determination of the angle of separation. The local pressures and the local Mach numbers determined in this way agree approximately with the values calculated from the cone angles of figure 6.

The transition Reynolds numbers evaluated in the above manner are shown in figure 10 plotted against the local Reynolds number per inch on the cone of separation. These transition Reynolds numbers are lower than the values expected for an attached boundary layer on a flat plate, but they increase with an increase in local stream Reynolds number per inch, in a fashion similar to that generally obtained for an attached boundary layer. At Reynolds numbers per inch below $0.1 \times 10^6$, the transition Reynolds numbers increase with an increase in spike length. This effect is in agreement with the trend shown in reference 16, where the stability of a laminar mixing layer increases with an increase in Mach number. At Reynolds numbers per inch above about $0.1 \times 10^6$, the transition Reynolds numbers for the flow over the spike with $L/D = 4$ begins to follow a different pattern. This flow characteristic may be a first indication of instability of the boundary layer on the spike ahead of separation at a stream Reynolds number based on the distance along the spike to separation of $0.31 \times 10^6$.

A cross plot of the data in figure 10 at four different Reynolds numbers is shown in figure 11 to allow a closer observation of the effect of local cone Mach number upon the transition Reynolds number. These data show the same trend as the data of reference 16. The comparison of the absolute level of the two sets of data should not be made, however, since two-dimensional flow is compared with conical flow, and this difference cannot necessarily be corrected by the Mangler transformation (ref. 26). Also, the flow conditions of reference 16 were evaluated just ahead of the start of separation, and the transition Reynolds numbers were based on the flow conditions and length of the separated layer just before any transition was noticed on the separated boundary. The data in figure 11, however, show the lower transition Reynolds numbers on the separated boundary at the lower Mach numbers and hint that at higher local Mach numbers the transition Reynolds numbers for separated flow and attached flow may approach the same value.

Some photographs of the flow around the smaller spiked body are shown in figure 4. It is difficult to see the start of transition with spike lengths of 1 and 2 diameters since the turbulent boundary is so fine that it is obscured by the background. The turbulent boundary can be easily seen in the flow for spike lengths of 3 and 4 diameters, and although some detail is lacking in the photographs of the smaller model, it appears that the flow fields are similar at the same stream Reynolds numbers based on diameter. Some measurements from schlieren photographs of the small model are shown in figures 5 to 10. These data show reasonable agreement with the data for the larger model, and show data in figure 10 for the spike length of 4 diameters at a higher unit Reynolds number than is possible with the larger model since the smaller model can be tested at these higher unit Reynolds numbers before transition takes place on the spike ahead of separation. It is then apparent that the sharp

change in trend seen in figures 5, 6, 8, and 9 would occur at a slightly higher Reynolds number for the smaller model.

As mentioned before, unsteady flow which appeared as a waviness of the boundaries and shocks was apparent in the schlieren pictures. Some of the boundaries were wavy when there was little evidence of transition, but this waviness seemed to be the first sign of instability on the separated boundary. The amplitude of the oscillation was much smaller and the frequency was much higher than that obtained from other investigations (refs. 6 and 7). Schlieren motion pictures taken at rates as high as 7,000 frames per second failed to show the unsteadiness except as fuzzy straight lines. The spark schlieren photographs which showed the waviness had a spark duration of approximately 3 microseconds.

L
2
4
8

## Pressure Distribution

The spike ahead of the stagnation point of the hemisphere affects the visible flow characteristics in the manner previously described. The effect of the altered flow characteristics upon the local pressure distribution is shown in figure 12 for different spike lengths and different Reynolds numbers. The pressure near the stagnation point is reduced by a factor of 4 by the shortest spike, and this pressure reduction increases with increasing spike lengths until the pressure is reduced by a factor of 25 in the case of the longest spike at the lowest Reynolds number. These pressures are well predicted by the ranges of the cone pressures taken from figure 8. The local pressure on the hemisphere increases from this cone value toward a maximum at the reattachment point, and then decreases rapidly after reattachment. This maximum pressure is similar to the stagnation point pressure with no spike when spike lengths of 1/2 diameter and 1 diameter are used. With increasingly longer spikes, the location of the peak pressure moves back as the location of reattachment moves back, and the maximum pressure at reattachment is reduced since the angle between the separated and solid boundaries is reduced, except when the shape of the separated region changes radically at higher Reynolds numbers for spike lengths of 4 diameters.

The spike reduced pressures on the cylinder by nearly 50 percent in some cases. The affected region on the cylinder is smaller with shorter spikes, however. The cylinder pressures were below the pressures obtained with no spike for about 1 diameter behind the hemisphere-cylinder juncture with the spike length of 1/2 diameter, and for about 2 diameters behind this juncture for the spike length of 1 diameter. The cylinder pressures with spike lengths of 2, 3, and 4 diameters were below the pressures with no spike over the entire cylinder. For comparison with cone-cylinder pressures, the pressure expected near the front of the cylinder with the overexpansion considered has been calculated for $M = 6.8$ by using cone theory and a two-dimensional expansion at the shoulder. As is shown in figure 12, although the measured pressure at the

hemisphere-cylinder juncture is, in general, lower than that for the unspiked body, it is not as low as the value obtained by this calculation.

The effect of Reynolds number on the pressure distribution over the model is greater near the location of reattachment and ahead of this point than over the remainder of the model. For the model with the spike length of 1/2 diameter, the pressure increases with Reynolds number at the 30° station (which is in the forward part of the reattachment region) as would be expected under the transitional boundary layer according to reference 16. With increasingly longer spikes, the station showing the expected variation of pressure is located farther from the stagnation point of the hemisphere. Some movement is observed in the location of reattachment as the Reynolds number changes, however, and part of the variation of pressure is caused by this movement, especially when the location of reattachment is very close to an orifice location and moves across it as the Reynolds number is varied. The spike causing the greatest variation in pressure with Reynolds number is the spike with $L/D = 4$ (fig. 12(e)). In this instance, it has been shown that the start of separation moves back along the spike as the Reynolds number is increased (fig. 5) and the angle of the start of separation varies by a factor of 4 (fig. 6), whereas for the other spike lengths the variation from a mean value is less than 20 percent. Notice that the pressure distribution for the spike length of 4 diameters at the highest Reynolds numbers agrees with the pressure distribution for the spike length of 1 diameter. The shape of the separated region was nearly the same in these two cases (as shown in figs. 5 and 6). No effect of the oscillation of the separated boundaries and shocks was noticed in the pressure measurements; probably the frequency of oscillation was too high for the frequency response of the pressure-measuring instruments.

The effect of the spike length upon the pressure drag of the hemisphere is shown in figure 13. The drag coefficient was determined by graphically integrating the areas under curves of the pressure coefficients plotted against $(r/R)^2$. It is apparent that the pressure drag of the hemisphere is reduced as the spike length is increased to 3 diameters. There is little change in the drag coefficient as the spike length is further increased to 4 diameters except in the case of Reynolds numbers above about $0.8 \times 10^6$. In this case the drag coefficient is associated with the sharp increase in the angle of the start of separation (fig. 6) and with the rapid retreat of position of the start of separation (fig. 5) caused by extensive transition of the attached boundary-layer on the spike at this Reynolds number. These results are in agreement with many of the findings of other investigations (refs. 1 to 9).

The drag coefficients are plotted as a function of Reynolds number in figure 14. These data show further the drag reduction caused by the increasing spike length and indicate the manner in which the drag coefficient increases as the Reynolds number is increased. This effect has

been shown previously in reference 7. This drag increase is caused by the expected increase in pressure under the transitional separated boundary as shown in reference 16. Again notice that the results for a spike length of 4 diameters become similar to those for a spike length of 1 diameter in the high Reynolds number range.

## Heat Transfer

The total heat transfer to a blunt nose has been increased by the addition of flow separation spikes under some conditions (ref. 3) and has been decreased by the addition of these spikes under other conditions (ref. 9). Theoretically (ref. 12) an increase in heat transfer might be expected for transitional or turbulent flow in the boundary layer over the separated region, since a large increase is predicted for lower Mach numbers. This result is contrary to the experimental results of reference 13, however. According to reference 12, a decrease in heat transfer should be expected for laminar flow over the entire separated region. In the present investigation, the range of test Reynolds numbers was such that it was possible to cover the range from laminar to turbulent flow over the separated region caused by the nose spikes.

The ratio of the local heat transfer with a spike to that expected at the stagnation point without a spike is shown in figure 15. Data taken with no spike are shown for comparison. The data shown for the unmodified hemisphere-cylinder are those obtained in the course of the present tests by the quasi-step start technique. The heat transfer is reduced near the base of the spike in all cases, but increases to a maximum near the point of reattachment to the hemisphere. This maximum value of heat transfer was below the no-spike stagnation-point value for the lowest Reynolds number tests with all the spikes, but the maximum value of heat transfer was from approximately 50 percent greater to double the no-spike stagnation-point value for the tests at the highest Reynolds numbers. From this maximum value the heat transfer falls rapidly over the remainder of the hemisphere nose and first part of the cylinder. The magnitude, the shape, and the correlation of this peak value with the location of reattachment suggest the start of a new boundary layer near the location of reattachment for theoretical consideration. Over the remainder of the cylinder the heat transfer either falls slowly, levels off, or increases in the fashion expected for the start of a transitional region.

An attempt was made to fit theory to the heat-transfer results of figure 15. Laminar-theory values were computed by the Stine and Wanlass method (ref. 28), which allows a transformation of an experimental pressure-gradient parameter to the corresponding incompressible flat-plate parameter by means of the Stewartson and Mangler transformations, and then allows the transformation of suitable incompressible flat-plate

heat-transfer parameters back to the compressible axisymmetric case by means of the same transformations. Turbulent-theory values were obtained from a method by Cohen, (ref. 29) in which the heat transfer was derived from the integrated equations of the boundary layer. The derivation utilized a Stewartson type transformation of the equations, the assumption of a quadratic dependence of total enthalpy upon velocity across the boundary layer (in which the coefficients of the velocity terms are functions of pressure gradient), and a compressibility correction for skin-friction coefficient based on flat-plate experimental data. The method was applied specifically for inverse-power-law velocity profiles and friction coefficients.

In both theories, the local heat transfer was computed by assuming the boundary layer to start at the apparent location of reattachment as seen from the schlieren photographs. The stagnation pressure and density of the flow after reattachment were calculated by considering the total-pressure loss at the nose of the spike, the total-pressure loss through the conical shock at separation, and the total-pressure loss through the oblique shock at reattachment. The recovery temperature was determined from the square root of the Prandtl number for the laminar-theory values and from the cube root of the Prandtl number for the turbulent-theory values. The stagnation-point heat transfer on the cylinder without a spike was computed from experimental results presented in reference 25.

The agreement between theoretical results and experimental data is not very close, but in general the trends indicated by the data are supported by the theoretical results. The theoretical calculations are very sensitive to pressure gradients, and part of the disagreement seen may be ascribed to slightly inaccurate pressure results used in the theories. It also appears that the agreement between theory and experiment could be enhanced in some cases by a small adjustment in the location of reattachment.

There is a noticeable dip in the heat transfer to the cylinder in the region immediately behind the hemisphere for spike lengths of 1 and 4 diameters (figs. 15(b) and (e)) at the highest Reynolds number and the heat transfer to the remainder of the cylinder suggests boundary-layer transition. A reexamination of figure 12 shows that the favorable pressure gradient shortly after reattachment is much greater for $L/D$ values of 1 and 4 at the highest Reynolds number tests than for the other tests. The reestablishment of a laminar boundary after transition has been studied both experimentally and theoretically on a $58^{\circ}$ cone-cylinder model in reference 30, and it appears that the effect shown in this reference may explain the dip in these data near the hemisphere-cylinder juncture. It is also noticed that the turbulent theory shows a dip near the dip seen in the data, which may provide an alternate explanation. This theory for the spike with $L/D = 1$ (fig. 15(b)), however, showed

an unrealistic small negative value of heat transfer over a small region. Thus, it is possible that the theory breaks down in this region. Therefore, the exact nature of the flow in this region is uncertain.

The effect of the variation of spike length upon the heat transfer is illustrated by replotting the data presented in figure 15 at approximately the same Reynolds number, and the results are shown in figure 16. The main effect is seen for the plot with the range $0.14 \times 10^6 \leqq R_D \leqq 0.16 \times 10^6$ (fig. 16(a)). This Reynolds number range is on the threshold necessary for pure laminar flow in the separated region. Thus, much of the variation in figure 16(a) is caused by the Reynolds number variation, since the condition of the boundary layer is very sensitive to the Reynolds number in this range. For the higher Reynolds number ranges of $0.33 \times 10^6 \leqq R_D \leqq 0.39 \times 10^6$ and $0.59 \times 10^6 \leqq R_D \leqq 0.66 \times 10^6$ the variation of heat transfer as a function of spike length is more noticeable near the nose of the configuration. The general consequence of lengthening the spike is a reduction of the heat transfer in the small area near the base of the spike, and an increase in the heat transfer after reattachment on the remainder of the hemisphere surface. At the higher test Reynolds numbers of $0.92 \times 10^6 \leqq R_D \leqq 1.05 \times 10^6$ and $1.2 \times 10^6 \leqq R_D \leqq 1.4 \times 10^6$ (figs. 16(d) and (e)), the dip in the heat transfer just behind the hemisphere-cylinder juncture suggesting the reestablishment of laminar flow in this region may be seen for the spike lengths of 1 and 4 diameters. The trend of local values of the heat transfer over the hemisphere are not as clearly seen for this range of Reynolds number.

The effect of the different spike lengths on the total heat transfer to the hemisphere nose is shown in figure 17. The total heat input to the hemisphere was evaluated by integrating curves of $q_s/q_{o,ns}$ plotted against the total area to the station. It is apparent that at high Reynolds numbers the heat transfer to the hemisphere is approximately doubled by the presence of the spike as has been reported in reference 3. The heat transfer decreases at reduced Reynolds numbers until the presence of the spike seemed to reduce the heat transfer by about 50 percent during tests at the lower Reynolds numbers. This agrees with the predictions of a reduced heat transfer under a separated boundary by the theory of reference 11, and with the reduced heat transfer to a spiked-nose body tested in helium at $M = 14$ and $R_D = 0.365 \times 10^6$ in reference 9.

Some interest has been shown in the ratio of drag to heat transfer since this is a measure of the effectiveness of aerodynamic braking in the atmosphere. The effect of the spike upon the ratios of the drag coefficient to the total heat input to the hemsiphere is shown in figure 18.

This ratio is reduced by the spike in all cases studied in this investigation. Thus, if a high drag to heat transfer ratio is desired for braking purposes at reentry into the atmosphere, the indication from these tests is that the spike is always detrimental. Similar results have also been mentioned by Bogdonoff and Vas (ref. 9), where at $M = 14$, $R_D = 0.365 \times 10^6$, and with a spike length of 4 diameters the heat-transfer coefficient was reduced to about 1/3 the no-spike value, while the drag coefficient was reduced to less than 1/10 the no-spike value.

## CONCLUDING REMARKS

In this investigation a spiked-nosed hemisphere-cylinder was tested at a nominal Mach number of 6.8 and in a free-stream Reynolds number range (based on the hemisphere diameter) of about $0.12 \times 10^6$ to $1.5 \times 10^6$ to determine the effect of the spike upon the shape and nature of the flow boundaries, the pressure distribution, and the aerodynamic heating over the model surface. This wide range of Reynolds numbers has allowed the investigation of the three cases of laminar, transitional, and turbulent flow over the separated boundaries.

The results of this investigation show that the heat transfer to the spiked-nosed hemisphere was greatly influenced by the type of flow over the separated boundary. The integrated heat transfer to the hemisphere was increased by the presence of the spike over the greater part of the Reynolds number range (between $0.3 \times 10^6$ and $1.5 \times 10^6$), but was decreased by the presence of the spike at the lowest Reynolds numbers (between $0.14 \times 10^6$ and $0.17 \times 10^6$). At the lowest Reynolds numbers the flow was laminar, although in some cases there was some evidence of transition at the location of reattachment. However, at the slightly higher Reynolds numbers (approx. $0.3 \times 10^6$), the start of transition was evident ahead of reattachment.

The pressure drag coefficient of the hemisphere-cylinder was reduced by all the spikes as has been observed by other investigators. As the spike length was increased, the drag coefficient was reduced until a minimum value was realized. Further increase in spike length caused an increase in drag coefficient when the Reynolds number was high enough to cause transition in the region of separation. The ratio of drag to heat transfer was reduced by the spike in every test, regardless of the spike length and location of transition.

The results for this three-dimensional axially symmetric body differ from findings for separation on a two-dimensional body in that some of the previously observed effects of the transitional separation were not

seen in the present tests until the start of transition was in the region of the start of separation or ahead of it. One of the major differences occurred when the start of separation continued to follow the laminar law instead of the transitional law as transition moved forward of the reattachment point.

The transition Reynolds numbers for the separated boundary layer were less than those for a solid boundary over the range of local Mach numbers used in the investigation. The transition Reynolds numbers based on local stream conditions over the region of separation increased with both an increasing Mach number and Reynolds number. It appeared that at increasing Mach numbers the transition Reynolds numbers for the separated boundary were approaching those for a solid boundary.

Langley Research Center,
National Aeronautics and Space Administration,
Langley Field, Va., August 11, 1959.

## REFERENCES


1. Jones, Jim J.: Flow Separation from Rods Ahead of Blunt Noses at Mach Number 2.72. NACA RM L52E05a, 1952.

2. Jones, Jim J.: Experimental Drag Coefficients of Round Noses with Conical Windshields at Mach Number 2.72. NACA RM L55E10, 1955.

3. Stalder, Jackson R., and Nielsen, Helmer V.: Heat Transfer from a Hemisphere-Cylinder Equipped with Flow-Separation Spikes. NACA TN 3287, 1954.

4. Moeckel, W. E.: Flow Separation Ahead of Blunt Bodies at Supersonic Speeds. NACA TN 2418, 1951.

5. Moeckel, W. E.: Flow Separation Ahead of a Blunt Axially Symmetric Body at Mach Numbers 1.75 to 2.10. NACA RM E51L25, 1951.

6. Beastall, D., and Turner, J.: The Effect of a Spike Protruding in Front of a Bluff Body at Supersonic Speeds. R. & M. No. 3007, British A.R.C., 1957.

7. Daniels, Lloyd E., and Yoshihara, Hideo: Effects of the Upstream Influence of a Shock Wave at Supersonic Speeds in the Presence of a Separated Boundary Layer. WADC Tech. Rep. No. 54-31, U.S. Air Force, Jan. 1954.

8. Mair, W. A.: Experiments on Separation of Boundary Layers on Probes in Front of Blunt-Nosed Bodies in a Supersonic Air Stream. Phil. Mag., ser. 7, vol. 43, no. 342, July 1952, pp. 695-716.

9. Bogdonoff, S. M., and Vas, I. E.: Preliminary Investigations of Spiked Bodies at Hypersonic Speeds. Rep. No. 412, (WADC TN 58-7, AD 142 280), Dept. Aero. Eng., Princeton Univ., Mar. 1958.

10. McMahon, Howard M.: An Experimental Study of the Effect of Mass Ejection at the Stagnation Point of a Blunt Body. Memo. No. 42, Hypersonic Res. Project, GALCIT, May 1, 1958.

11. Hartley, Richard M.: Leading-Edge Spikes to Reduce the Drag of Wings at Supersonic Airspeeds. Aero Rep 925, David Taylor Model Basin, Navy Dept., Sept. 1957.

12. Chapman, Dean R.: A Theoretical Analysis of Heat Transfer in Regions of Separated Flow. NACA TN 3792, 1956.

13. Larson, Howard K.: Heat Transfer in Separated Flows. Rep. No. 59-37, Inst. Aero. Sci., Jan. 1959.

14. Love, Eugene S.: Pressure Rise Associated with Shock-Induced Boundary Layer Separation. NACA TN 3601, 1955.

15. Bogdonoff, S. M., and Kepler, C. E., and Sanlorenzo, E.: A Study of Shock Wave Turbulent Boundary Layer Interaction at M = 3. Rep. No. 222, (Contract No. N6-onr-270, Task Order No. 6, Project No. NR-061-049), Dept. Aero. Eng., Princeton Univ., July 1953.

16. Chapman, Dean R., Kuehn, Donald M., and Larson, Howard K.: Investigation of Separated Flows in Supersonic and Subsonic Streams With Emphasis on the Effect of Transition. NACA Rep. 1356, 1958. (Supersedes NACA TN 3869.)

17. Bernstein, Harry, and Brunk, William E.: Exploratory Investigation in the Separated Region Ahead of Two Blunt Bodies at Mach Number 2. NACA RM E55D07b, 1955.

18. Gadd, D. E., Holder, D. W., and Regan, J. D.: An Experimental Investigation of the Interaction Between Shock Waves and Boundary Layers. Proc. Roy. Soc. (London), ser. A, vol. 226, no. 1165, Nov. 9, 1954, pp. 227-253.

19. Holder, D. W., Chinneck, A., and Gadd, G. E.: An Experimental Investigation of the Interaction of a Shock Wave with a Subsonic Stream Bounded by a Wall. Phil. Mag., ser. 7, vol. 45, no. 369, Oct. 1954, pp. 997-1009.

20. Gadd, G. E.: An Experimental Investigation of Heat Transfer Effects on Boundary Layer Separation in Supersonic Flow. Jour. Fluid Mech., vol. 2, pt. 2, Mar. 1957, pp. 105-122.

21. Czarnecki, K. R., and Sinclair, Archibald R.: A Note on the Effect of Heat Transfer on Peak Pressure Rise Associated with Separation of Turbulent Boundary Layer on a Body of Revolution (NACA RM-10) at a Mach Number of 1.61. NACA TN 3997, 1957.

22. Gadd, G. E.: Interactions Between Wholly Laminar or Wholly Turbulent Boundary Layers and Shock Waves Strong Enough to Cause Separation. Jour. Aero. Soc., vol. 20, no. 11, Nov. 1953, pp. 729-739.

23. McLellan, Charles H., Williams, Thomas W., and Bertram, Mitchel H.: Investigation of a Two-Step Nozzle in the Langley 11-Inch Hypersonic Tunnel. NACA TN 2171, 1950.

L
2
4
8

24. McLellan, Charles H., Williams, Thomas W., and Beckwith, Ivan E.: Investigation of the Flow Through A Single-Stage Two-Dimensional Nozzle in the Langley 11-Inch Hypersonic Tunnel. NACA TN 2223, 1950.

25. Crawford, Davis H., and McCauley, William D.: Investigation of the Laminar Aerodynamic Heat-Transfer Characteristics of a Hemisphere-Cylinder in the Langley 11-Inch Hypersonic Tunnel at a Mach Number of 6.8. NACA Rep. 1323, 1957. (Supersedes NACA TN 3706.)

26. Bertram, Mitchel H.: Exploratory Investigation of Boundary-Layer Transition on a Hollow Cylinder at a Mach Number of 6.9. NACA Rep. 1313, 1957. (Supersedes NACA TN 3546.)

27. Tetervin, Neal: Remarks Concerning Transition Reynolds Numbers on Cones and Flat Plates. Jour. Aero. Sci. (Readers Forum), vol. 24, no. 7, July 1957, pp. 545-546.

28. Stine, Howard A., and Wanlass, Kent: Theoretical and Experimental Investigation of Aerodynamic-Heating and Isothermal Heat-Transfer Parameters on a Hemispherical Nose With Laminar Boundary Layer at Supersonic Mach Numbers. NACA TN 3344, 1954.

29. Cohen, Nathaniel B.: A Method for Computing Turbulent Heat Transfer in the Presence of a Streamwise Pressure Gradient for Bodies in High-Speed Flow. NASA MEMO 1-2-59L, 1959.

30. Sternberg, Joseph: The Transition From a Turbulent to a Laminar Boundary Layer. Rep. No. 906, Ballistic Res. Labs., Aberdeen Proving Ground, May 1954.

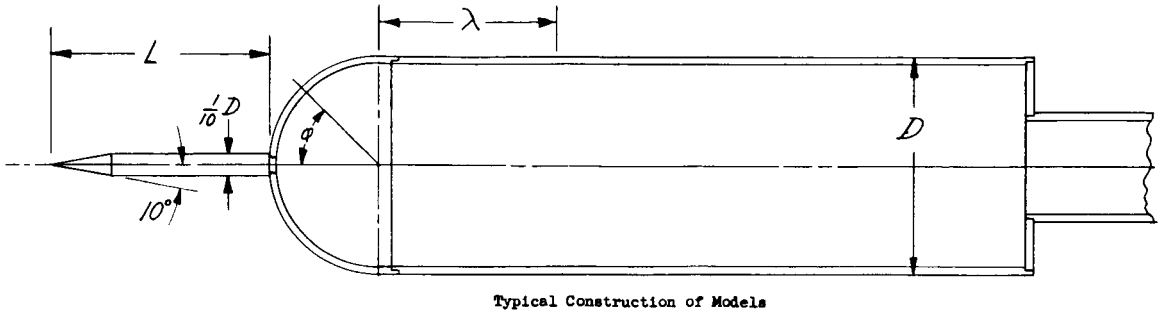


Typical Construction of Models

Orifice and Thermocouple Locations

| Pressure model (3.000-inch O. D.) | | | | Heat-transfer model (3.025-inch O. D.) | | | |
|---|---|---|---|---|---|---|---|
| Hemisphere | | Cylinder | | Hemisphere | | Cylinder | |
| Station | φ, deg | Station | λ, in. | Station | φ, deg | Station | λ, in. |
| 1 | 0 | 8 | 0.393 | 1 | 0 | 12 | 0.131 |
| 2 | 15 | 9 | .785 | 2 | 5 | 13 | .50 |
| 3 | 30 | 10 | 1.50 | 3 | 10 | 14 | .75 |
| 4 | 45 | 11 | 3.00 | 4 | 20 | 15 | 1.00 |
| 5 | 60 | 12 | 6.00 | 5 | 30 | 16 | 1.50 |
| 6 | 75 | 13 | 7.50 | 6 | 45 | 17 | 2.00 |
| 7 | 90 | 14 | 8.50 | 7 | 60 | 18 | 3.00 |
| | | | | 8 | 70 | 19 | 4.00 |
| | | | | 9 | 80 | 20 | 5.00 |
| | | | | 10 | 85 | 21 | 6.00 |
| | | | | 11 | 90 | 22 | 7.00 |
| | | | | | | 23 | 7.50 |
| | | | | | | 24 | 8.00 |
| | | | | | | 25 | 8.50 |

Figure 1.- Construction and instrumentation details of heat-transfer and pressure models.

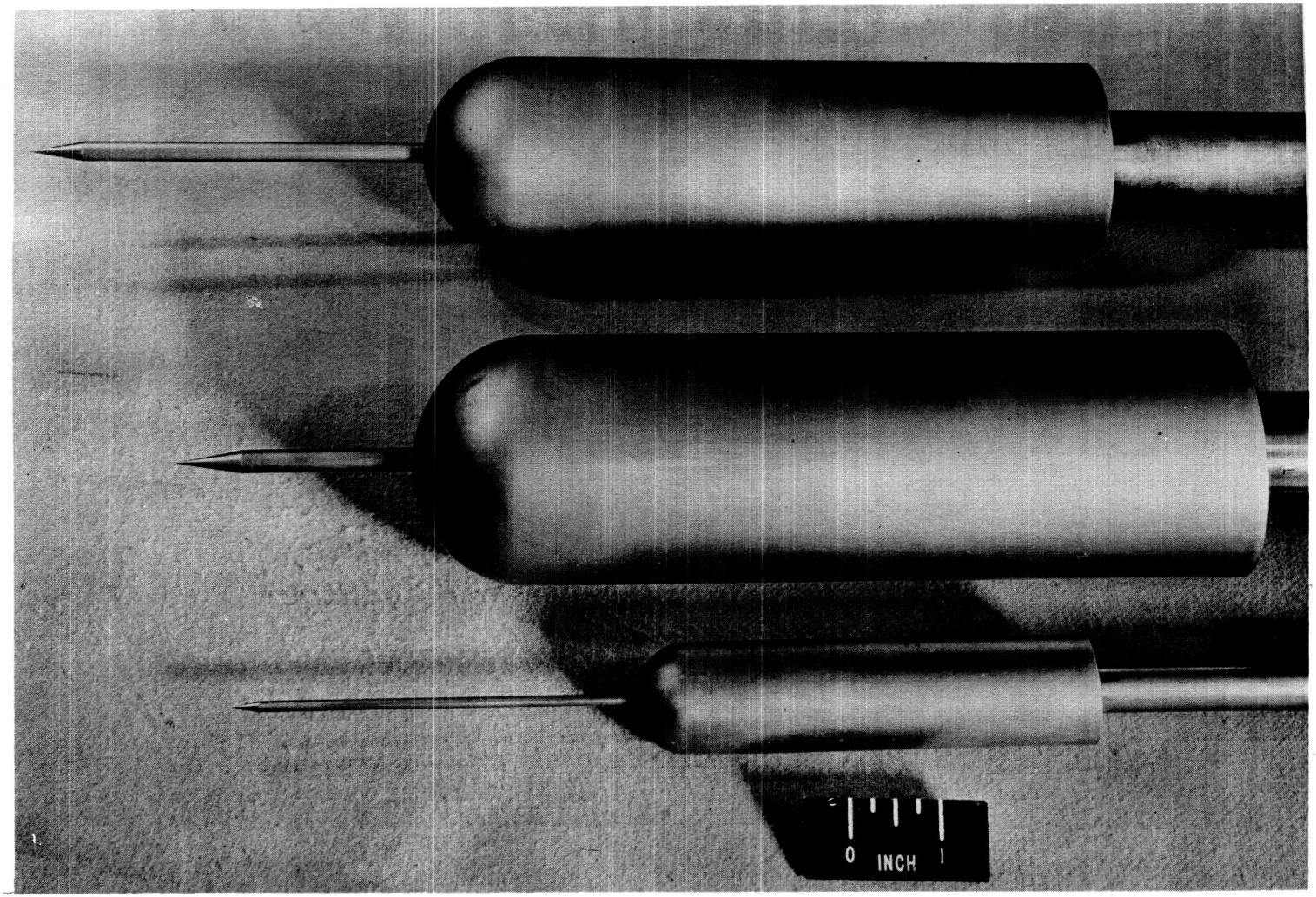


Figure 2.- Spike-nosed hemisphere-cylinder models. L-58-404a

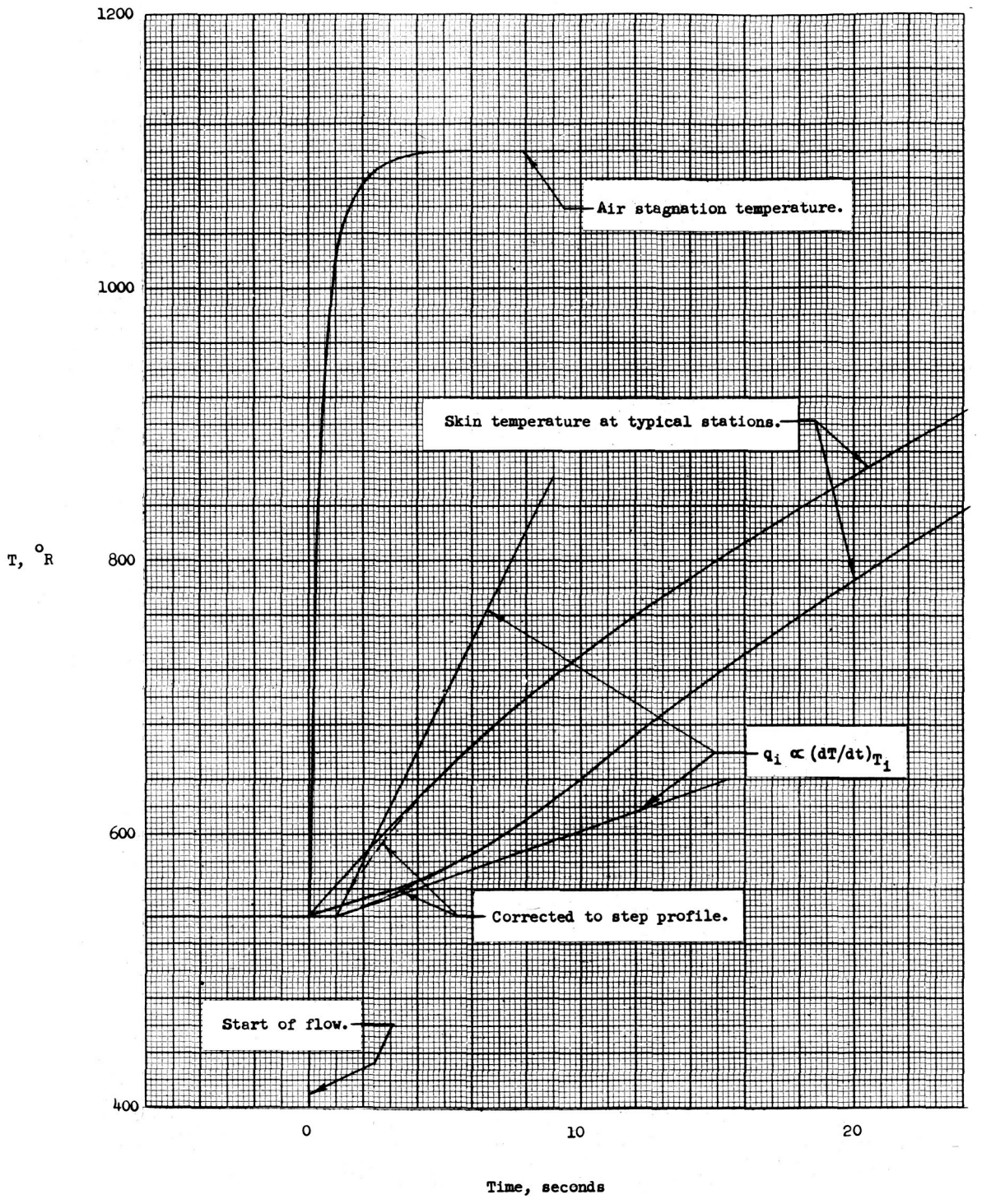


Figure 3.- Method of heat-transfer measurement.

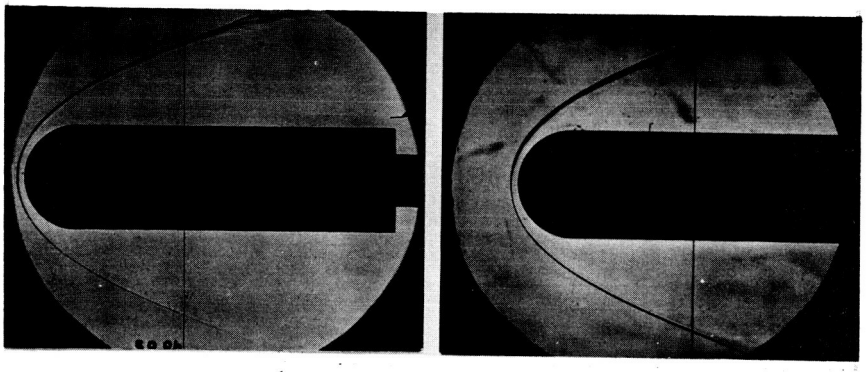

$R_D = 0.52 \times 10^6$ (a) 3" Dia.; L/D = 0. $R_D = 1.1 \times 10^6$

(a) 3-inch diameter; L/D = 0.



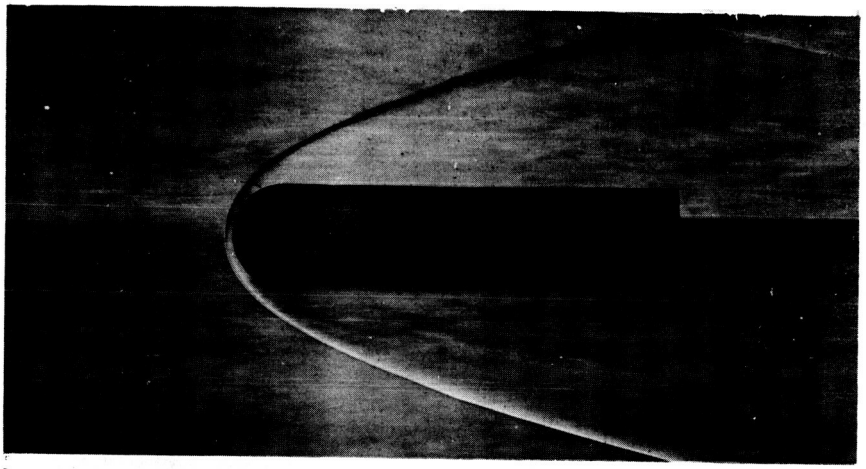

$R_D = 0.50 \times 10^6$

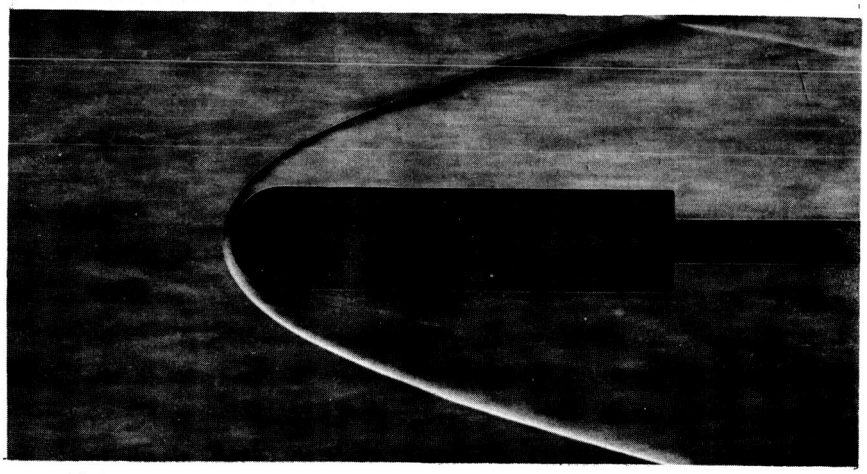

$R_D = 0.29 \times 10^6$

(b) 1.17-inch diameter; L/D = 0.

L-59-5054

Figure 4.- Flow characteristics of spiked-nose hemisphere cylinder.

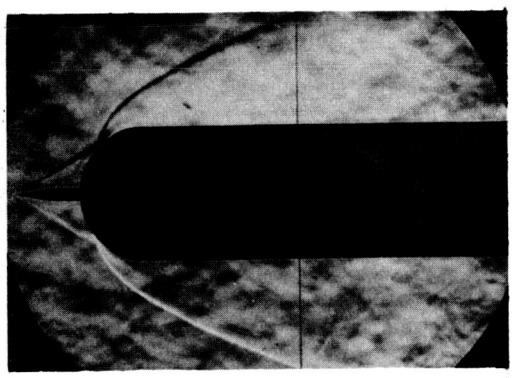

$R_D = 0.14 \times 10^6$

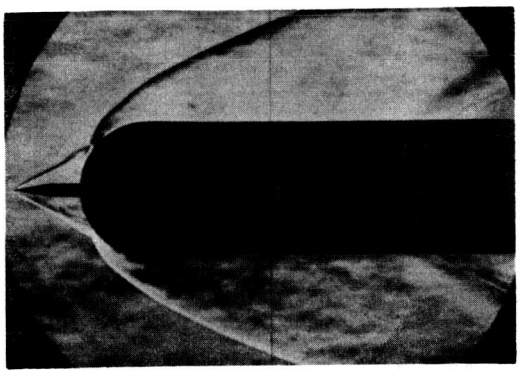

$R_D = 0.92 \times 10^6$

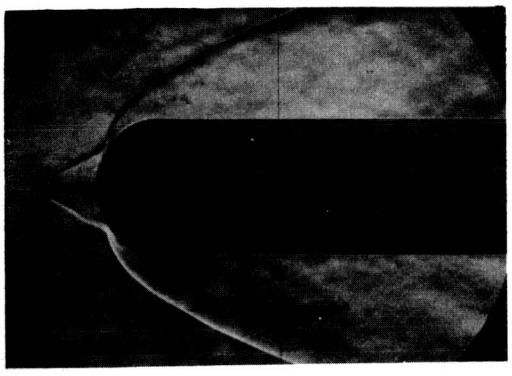

$R_D = 0.32 \times 10^6$

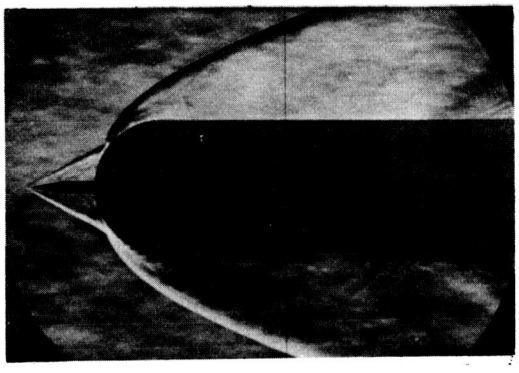

$R_D = 1.3 \times 10^6$

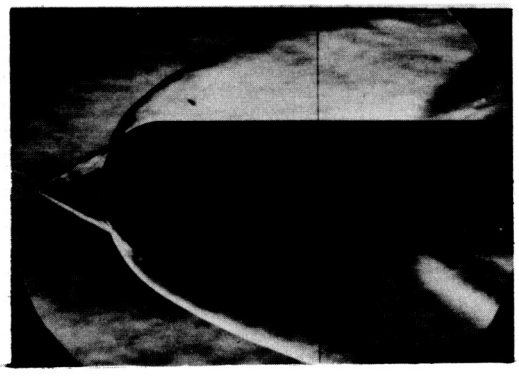

$R_D = 0.61 \times 10^6$

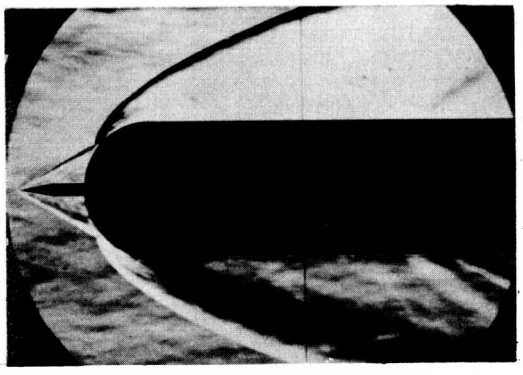

$R_D = 1.4 \times 10^6$

(c) 3-inch diameter; L/D = 1/2. L-59-5055

Figure 4.- Continued.

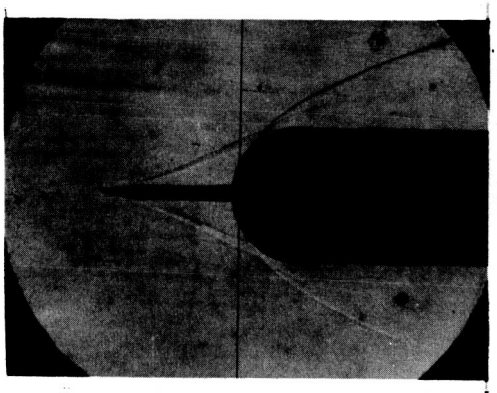

$R_D = 0.13 \times 10^6$

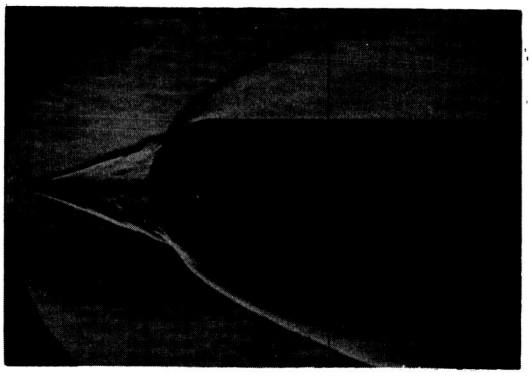

$R_D = 0.84 \times 10^6$

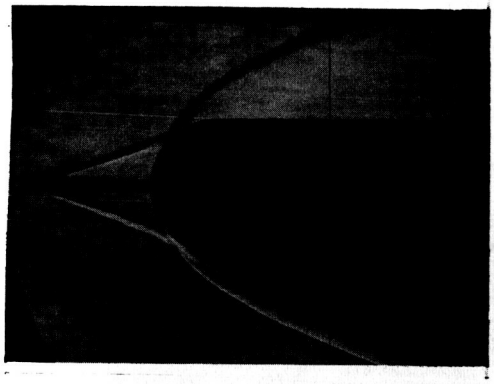

$R_D = 0.33 \times 10^6$

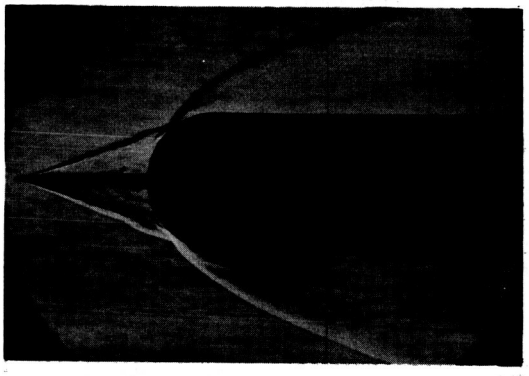

$R_D = 1.2 \times 10^6$

$R_D = 0.59 \times 10^6$

$R_D = 1.5 \times 10^6$

(d) 3-inch diameter; L/D = 1. L-59-5056

Figure 4.- Continued.

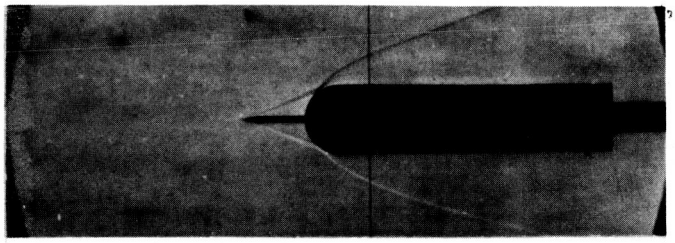

$R_D = 0.06 \times 10^6$

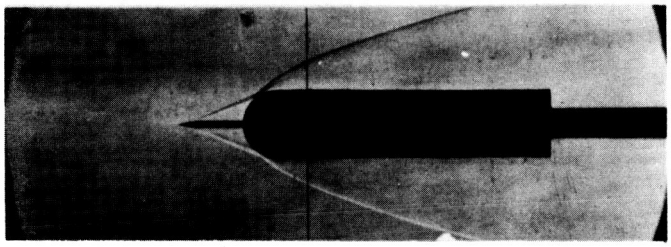

$R_D = 0.11 \times 10^6$

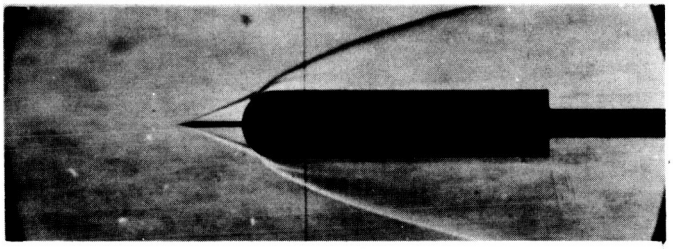

$R_D = 0.23 \times 10^6$

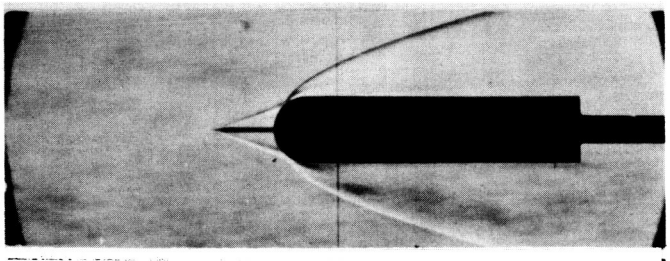

$R_D = 0.43 \times 10^6$

(e) 1.17-inch diameter; L/D = 1. L-59-5057

Figure 4.- Continued.

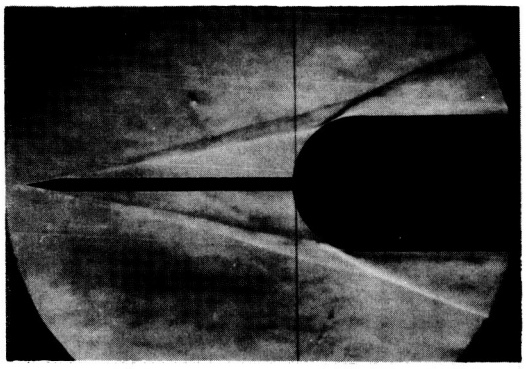

$R_D = 0.15 \times 10^6$

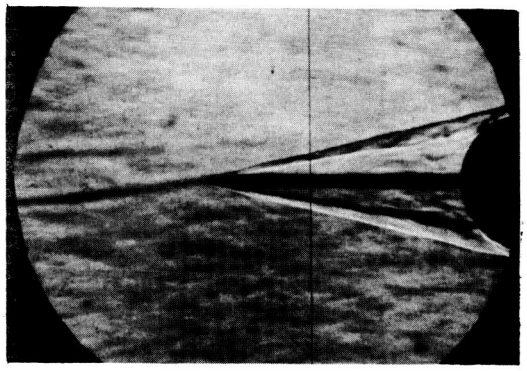

$R_D = 0.69 \times 10^6$

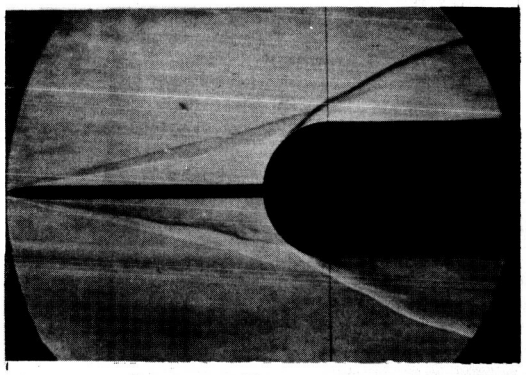

$R_D = 0.34 \times 10^6$

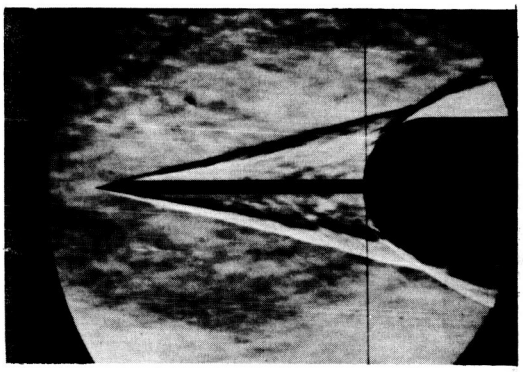

$R_D = 0.95 \times 10^6$

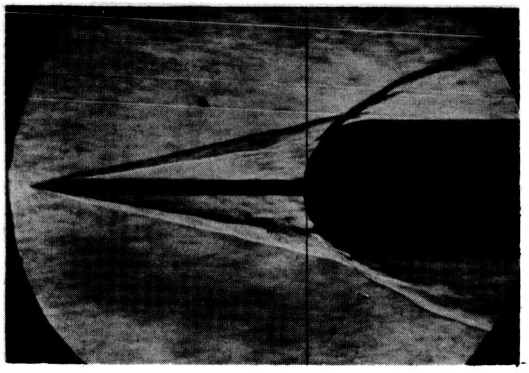

$R_D = 0.60 \times 10^6$

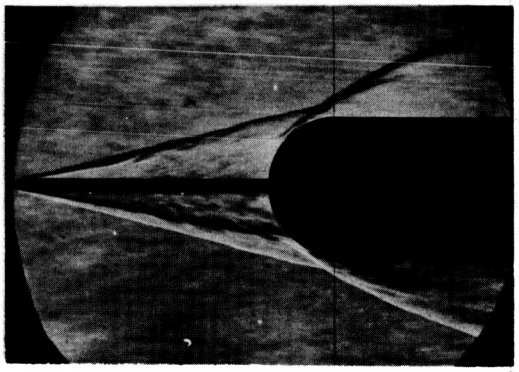

$R_D = 1.2 \times 10^6$

(f) 3-inch diameter; L/D = 2. L-59-5058

Figure 4.- Continued.

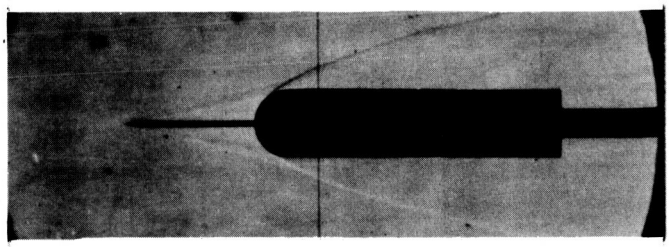

$R_D = 0.06 \times 10^6$

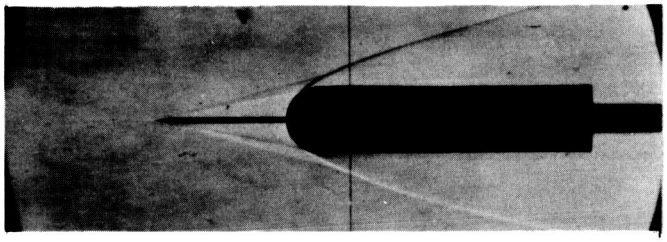

$R_D = 0.12 \times 10^6$

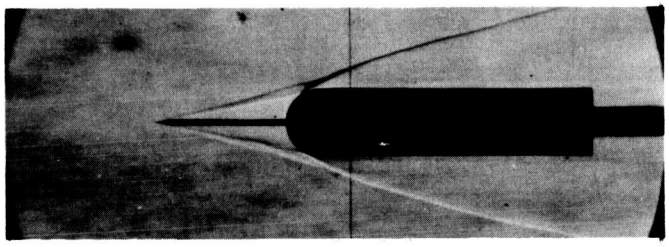

$R_D = 0.23 \times 10^6$

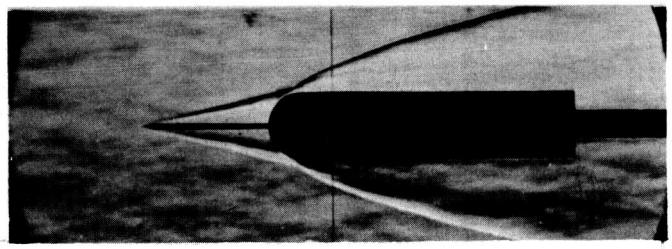

$R_D = 0.50 \times 10^6$

(g) 1.17-inch diameter; L/D = 2. L-59-5059

Figure 4.- Continued.

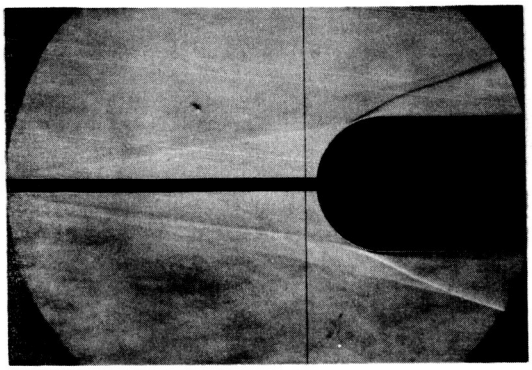

$R_D = 0.14 \times 10^6$

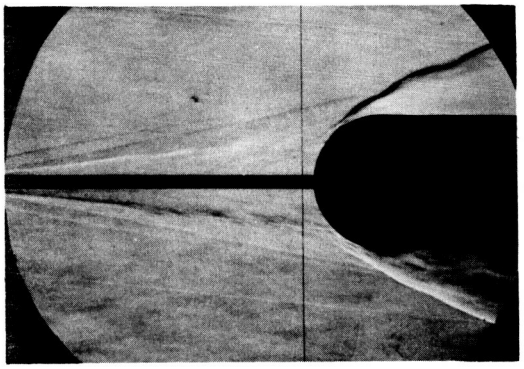

$R_D = 0.60 \times 10^6$

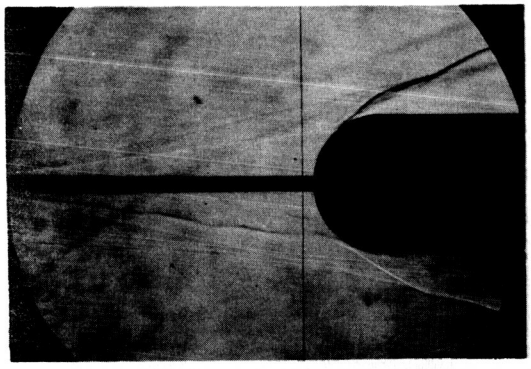

$R_D = 0.26 \times 10^6$

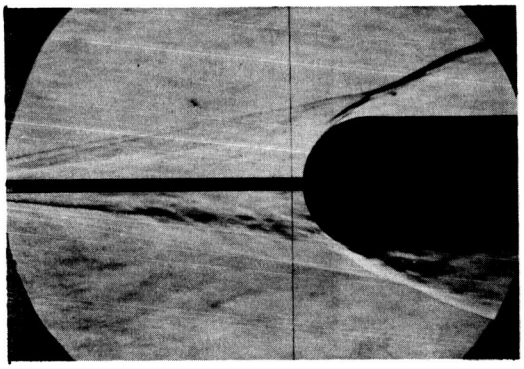

$R_D = 0.90 \times 10^6$

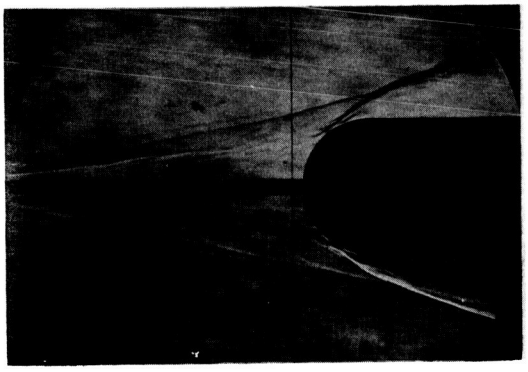

$R_D = 0.45 \times 10^6$

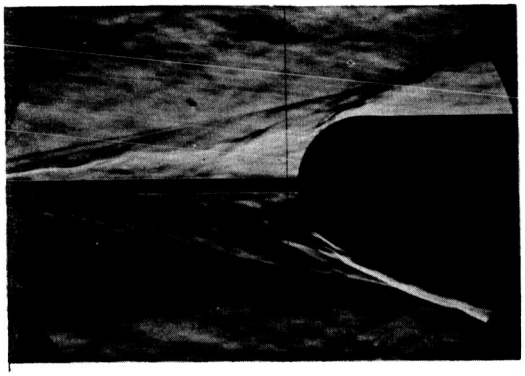

$R_D = 1.2 \times 10^6$

(h) 3-inch diameter; L/D = 3. L-59-5060

Figure 4.- Continued.

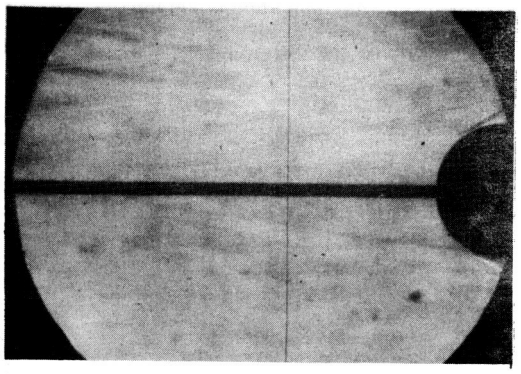

$R_D = 0.13 \times 10^6$

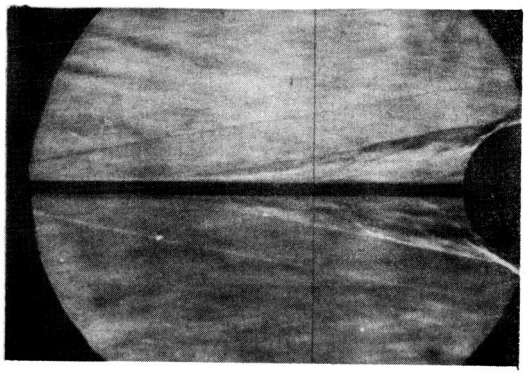

$R_D = 0.75 \times 10^6$

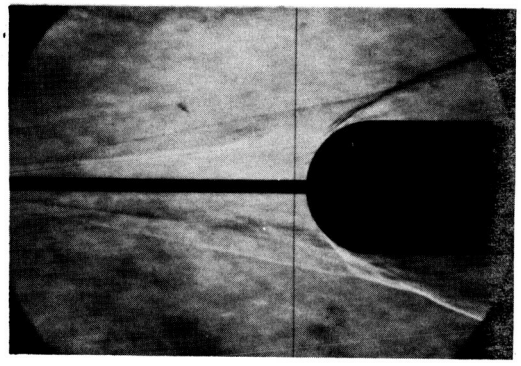

$R_D = 0.36 \times 10^6$

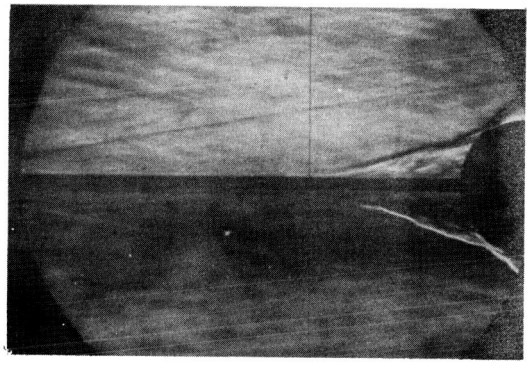

$R_D = 1.0 \times 10^6$

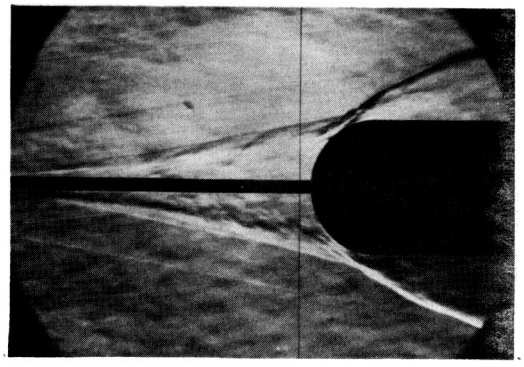

$R_D = 0.59 \times 10^6$

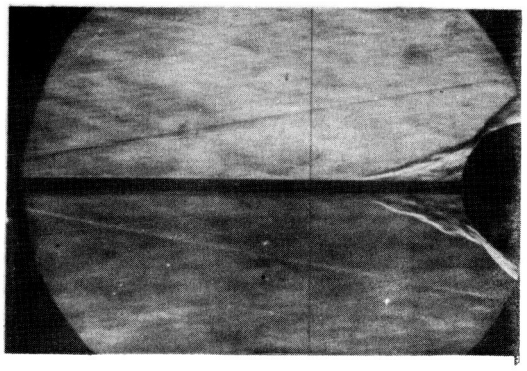

$R_D = 1.3 \times 10^6$

(i) 3-inch diameter; L/D = 4. L-59-5061

Figure 4.- Continued.

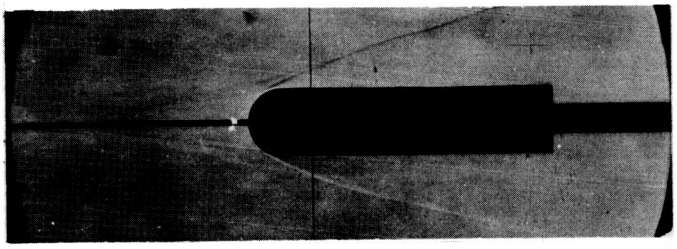

$R_D = 0.07 \times 10^6$

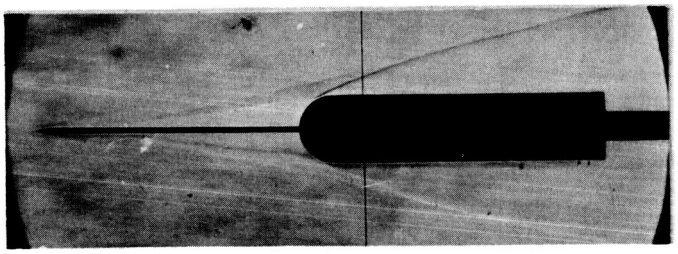

$R_D = 0.12 \times 10^6$

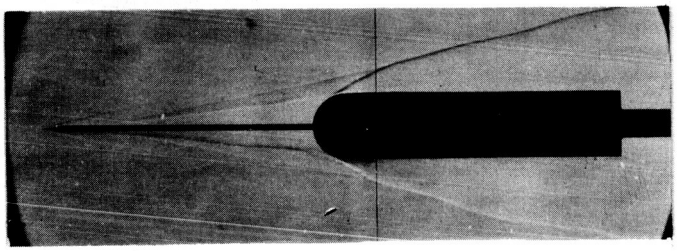

$R_D = 0.21 \times 10^6$

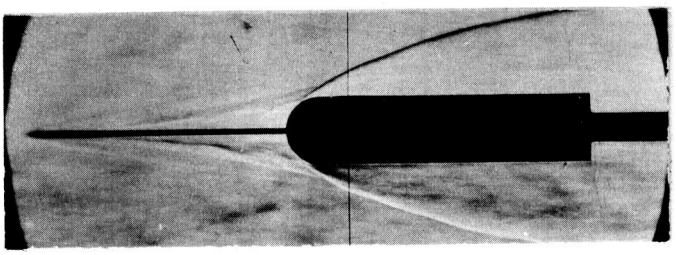

$R_D = 0.49 \times 10^6$

(j) 1.17-inch diameter; L/D = 4. L-59-5062

Figure 4.- Concluded.

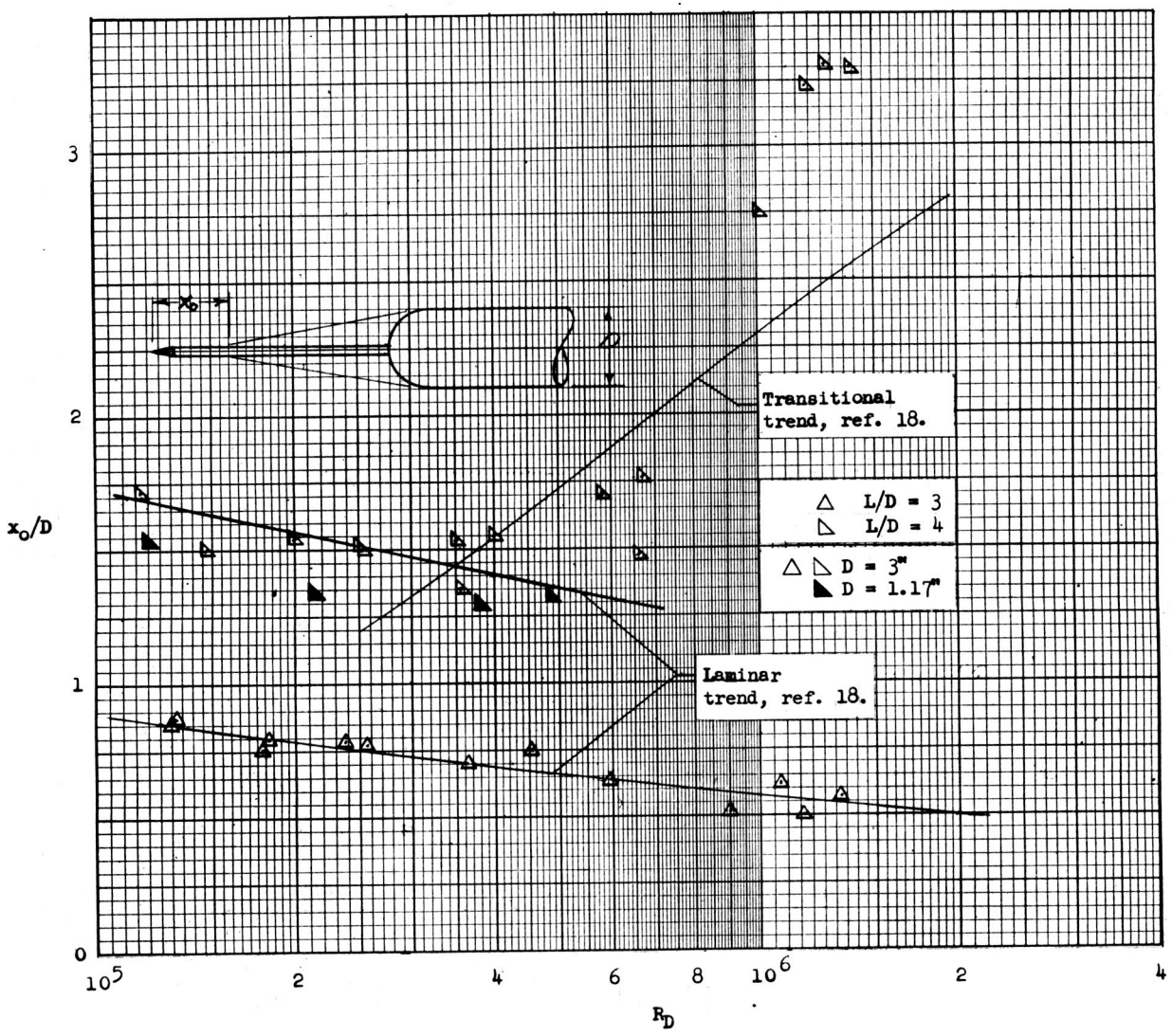


Figure 5.- Effect of Reynolds number upon movement of start of separation on spikes with L/D = 3 and L/D = 4.

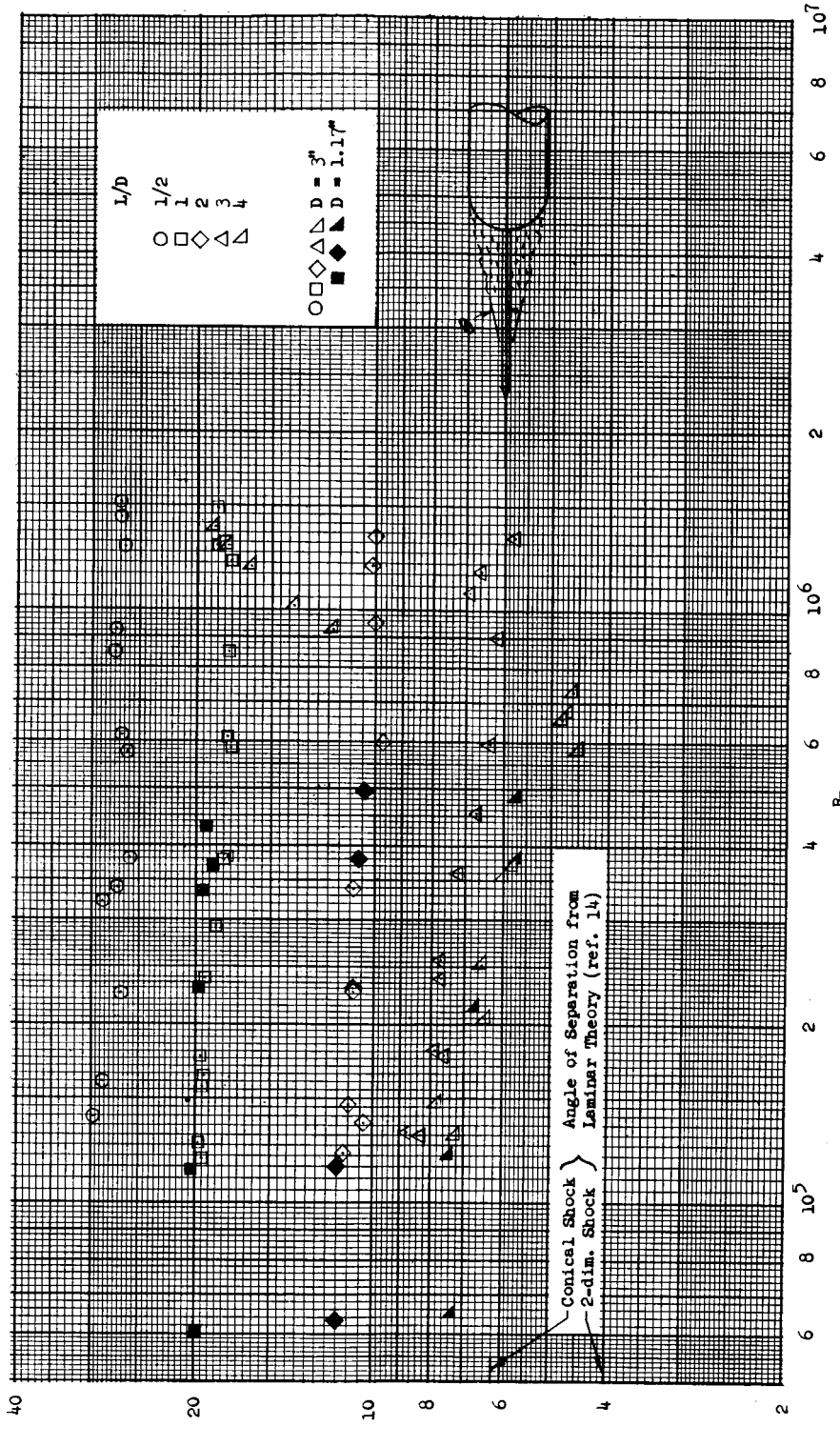


Figure 6.- Effect of spike length and Reynolds number upon conical half-angle of separation.

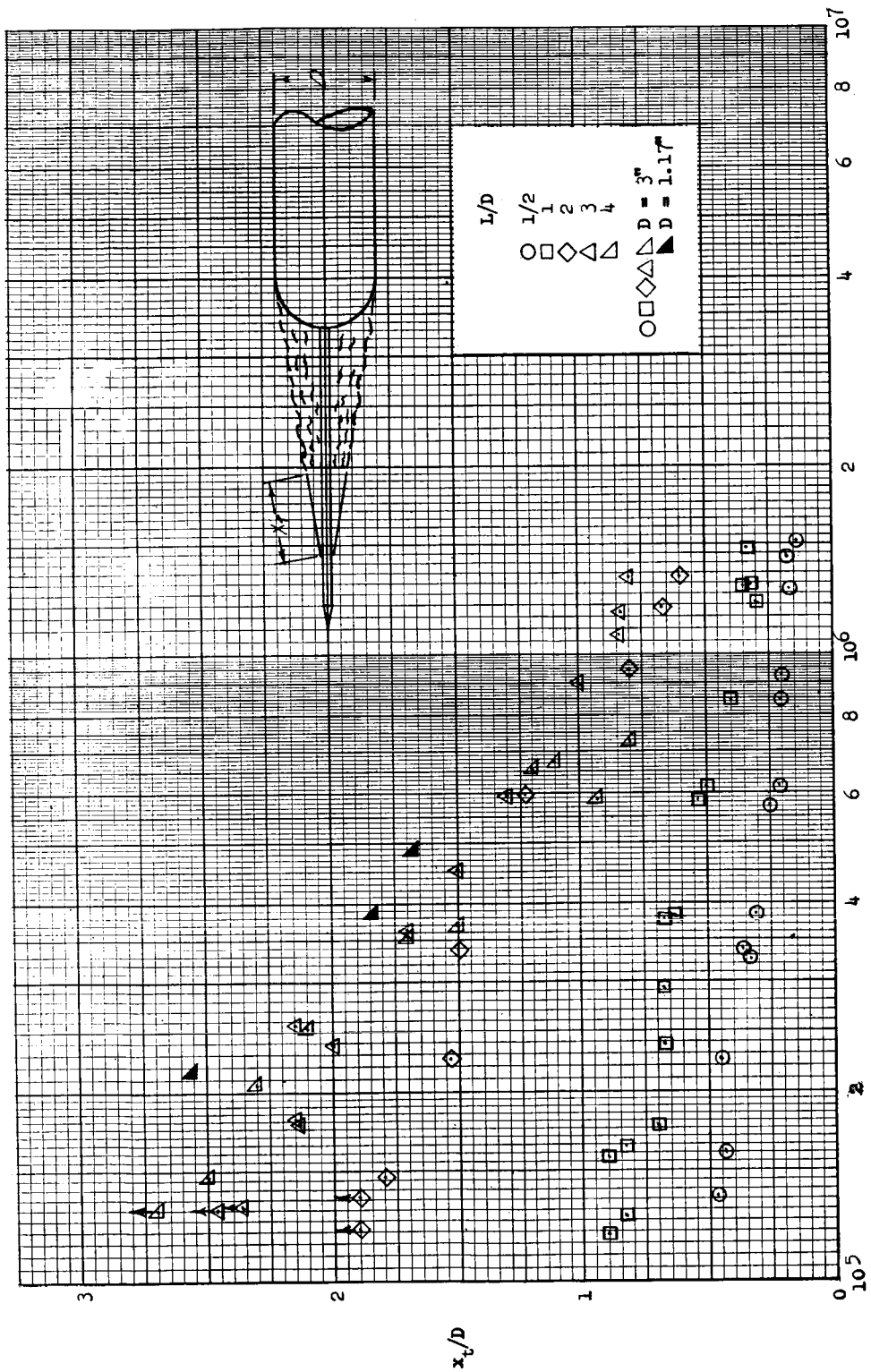


Figure 7.- Effect of spike length and Reynolds number upon the separated boundary-layer length to transition. Arrows indicate transition value higher than plotted value.

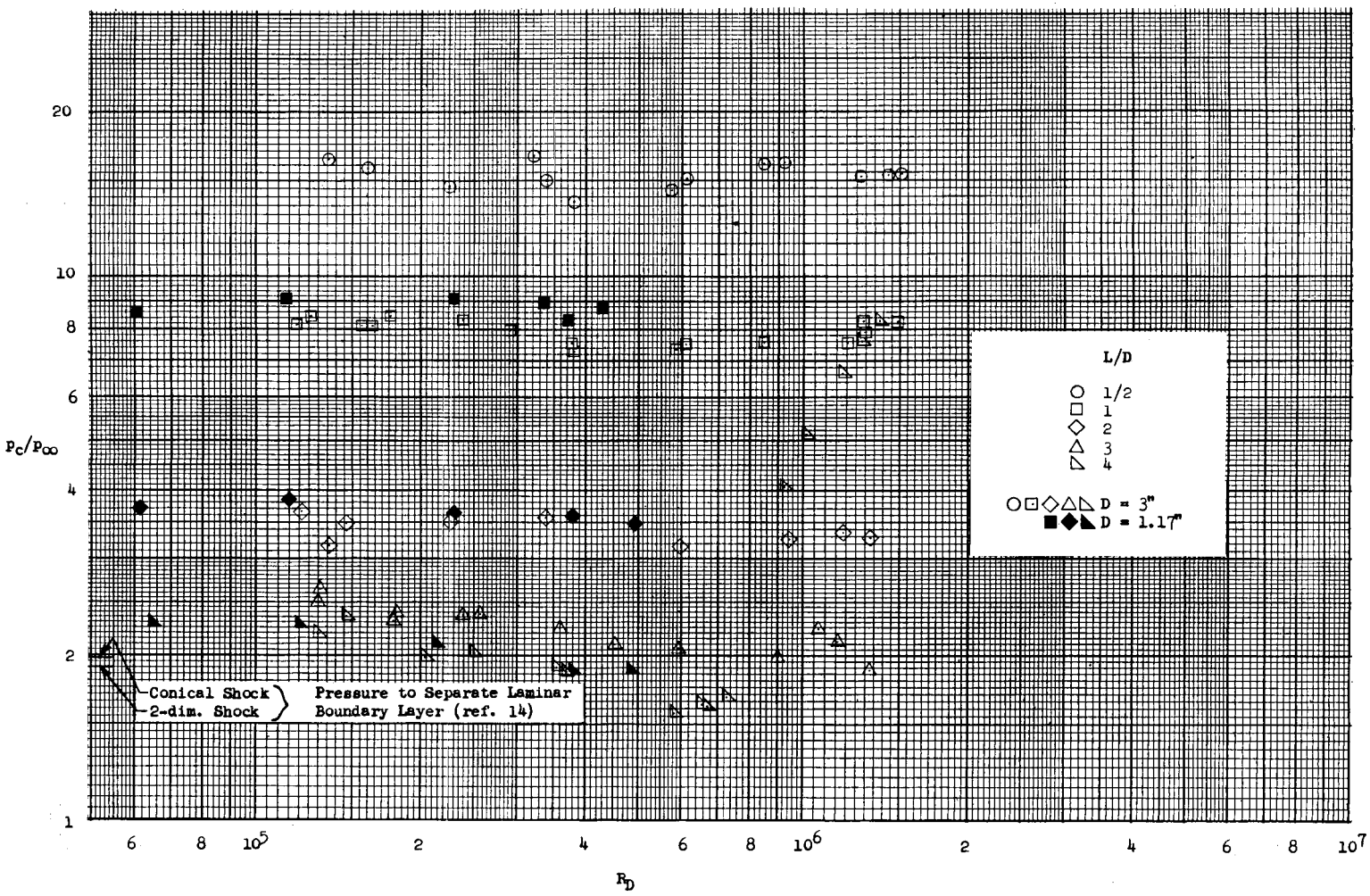


Figure 8.- Calculated local to stream pressure ratios on the conical separated boundaries.

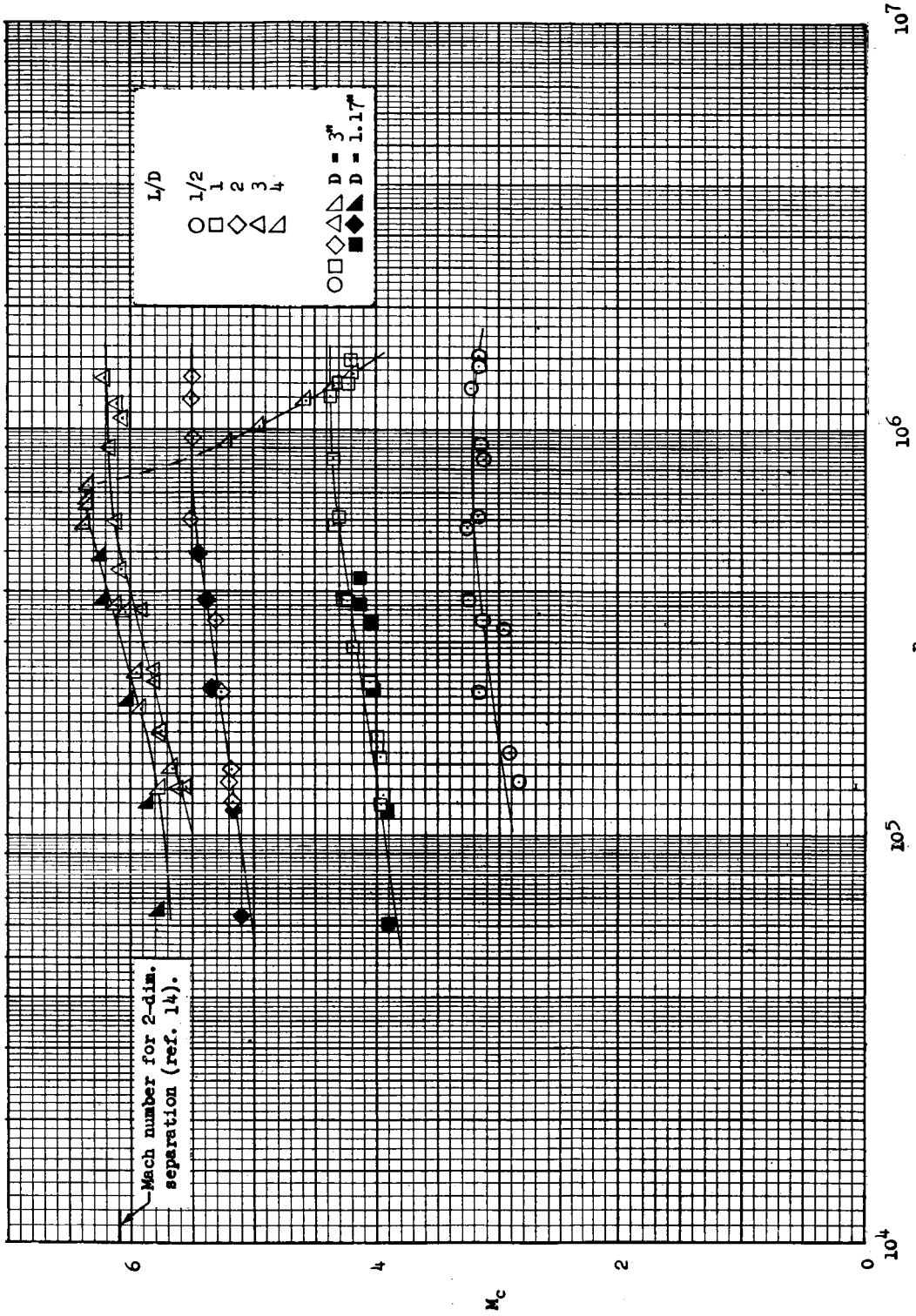


Figure 9.- Calculated local cone Mach numbers along the separated boundaries.

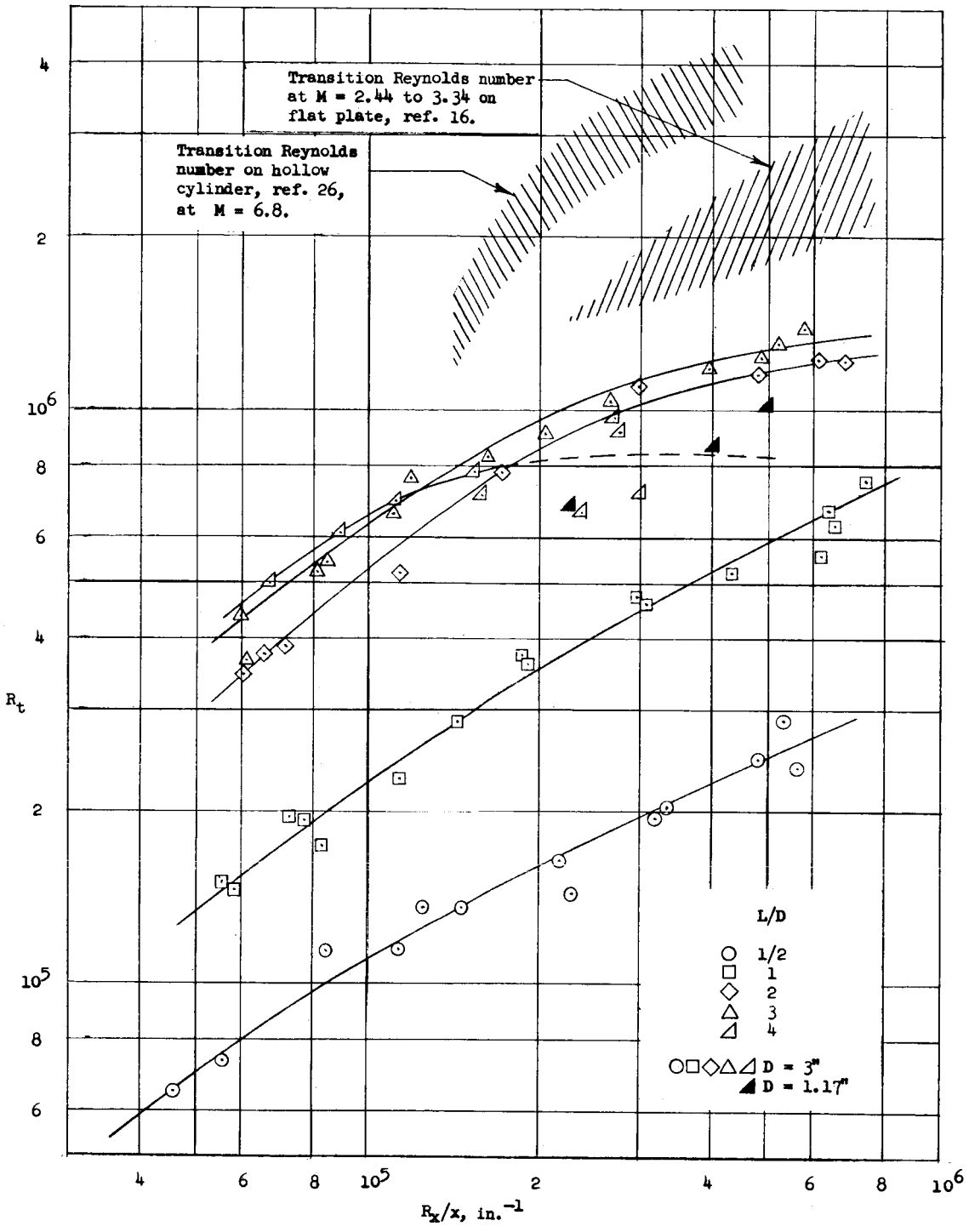


Figure 10.- Effect of spike length and local cone Reynolds number upon Reynolds number to transition along separated boundary.

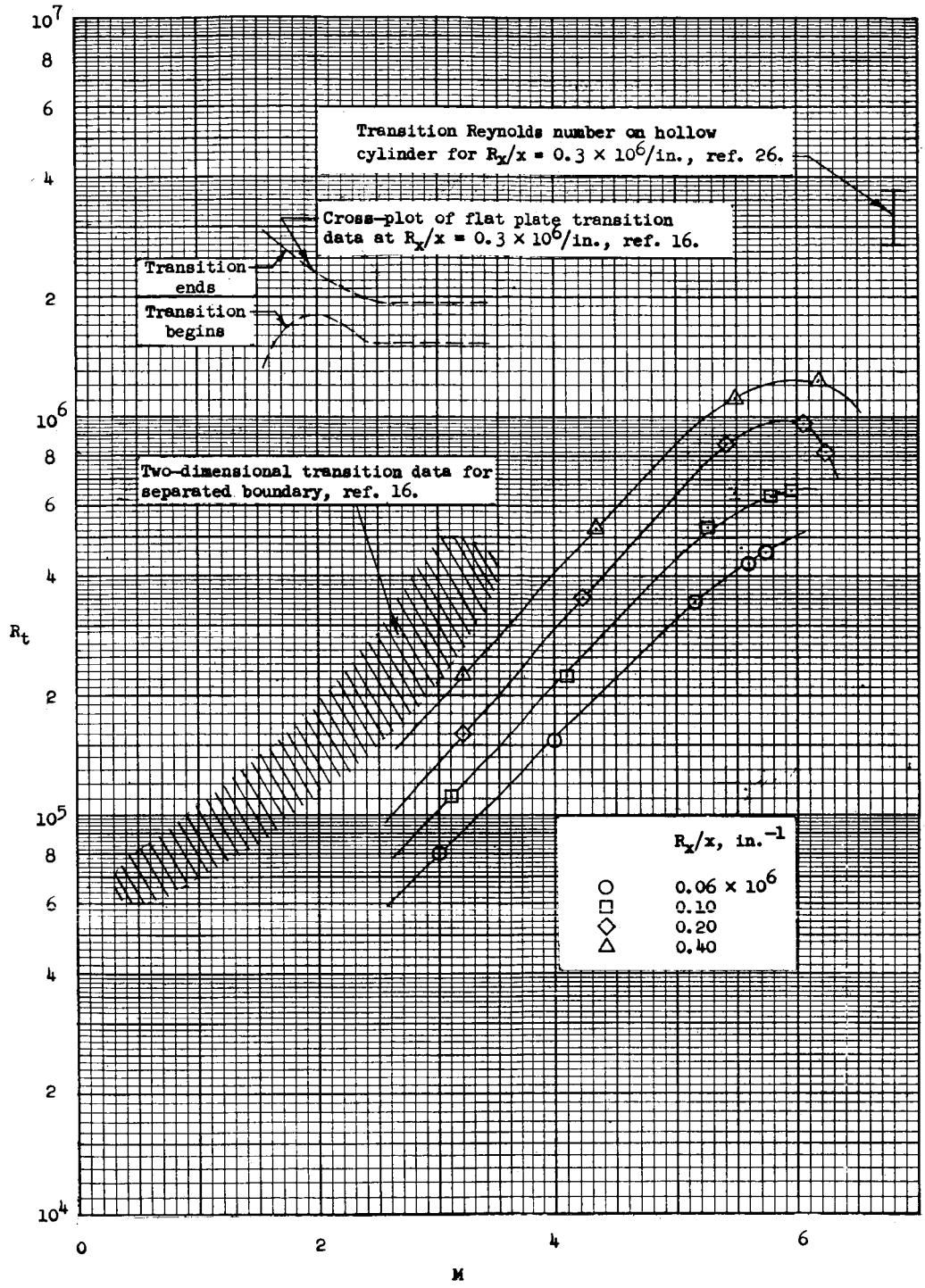


Figure 11.- Effect of local cone Mach number upon transition Reynolds number for separated boundary.

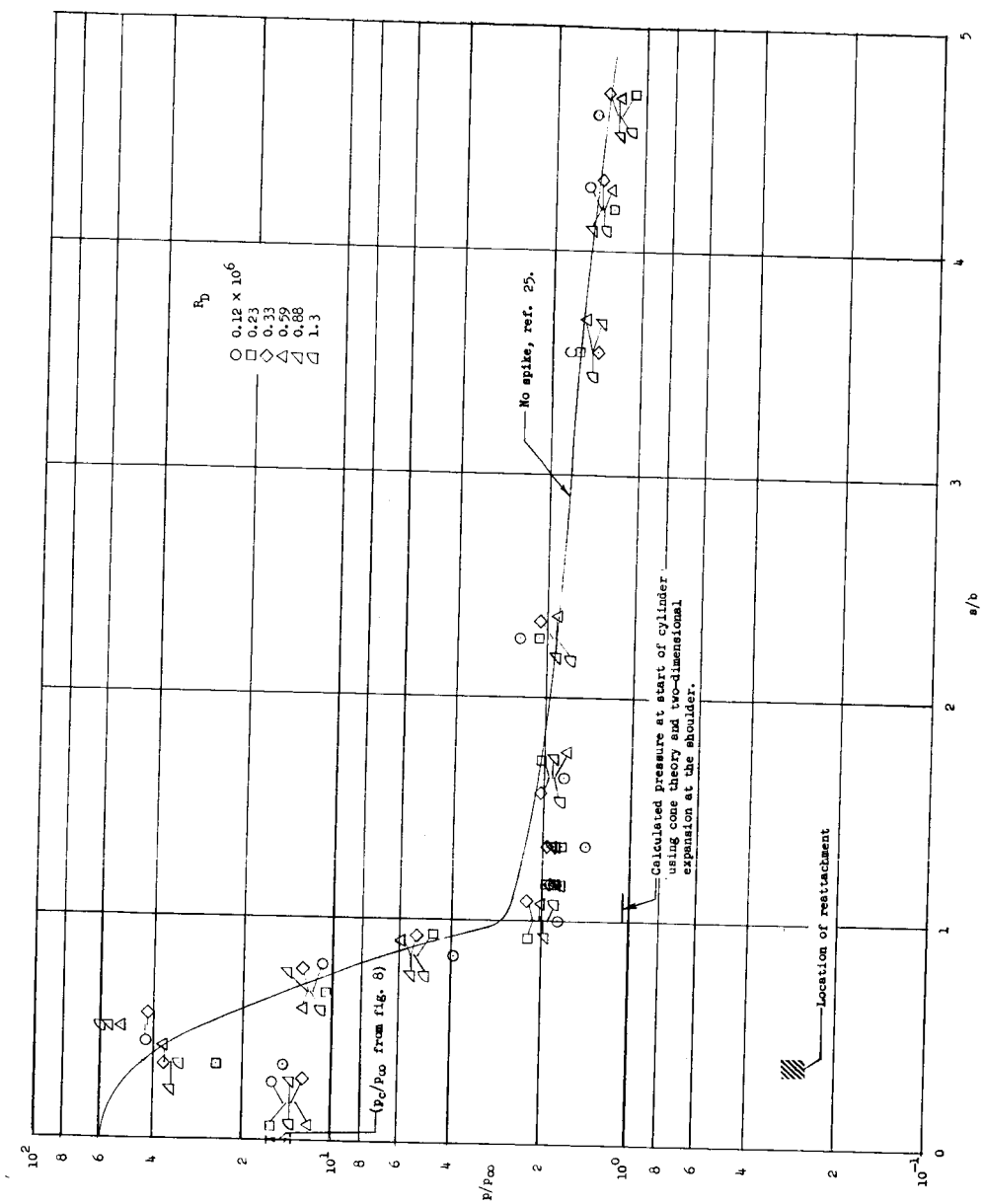


(a) L/D = 1/2.

Figure 12.- Effect of spike length and Reynolds number upon the local pressure distribution on the hemisphere-cylinder.

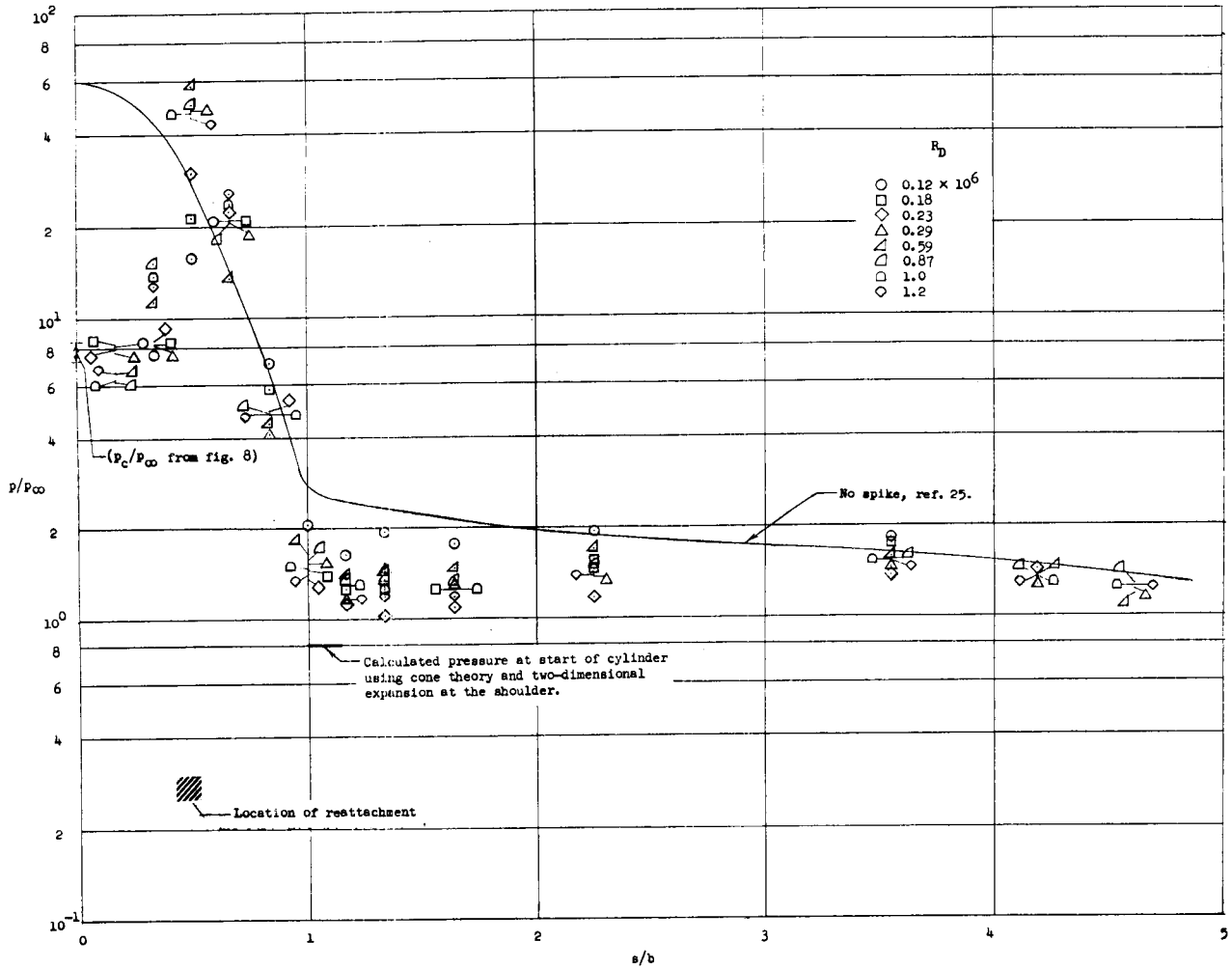


(b) L/D = 1.

Figure 12.- Continued.

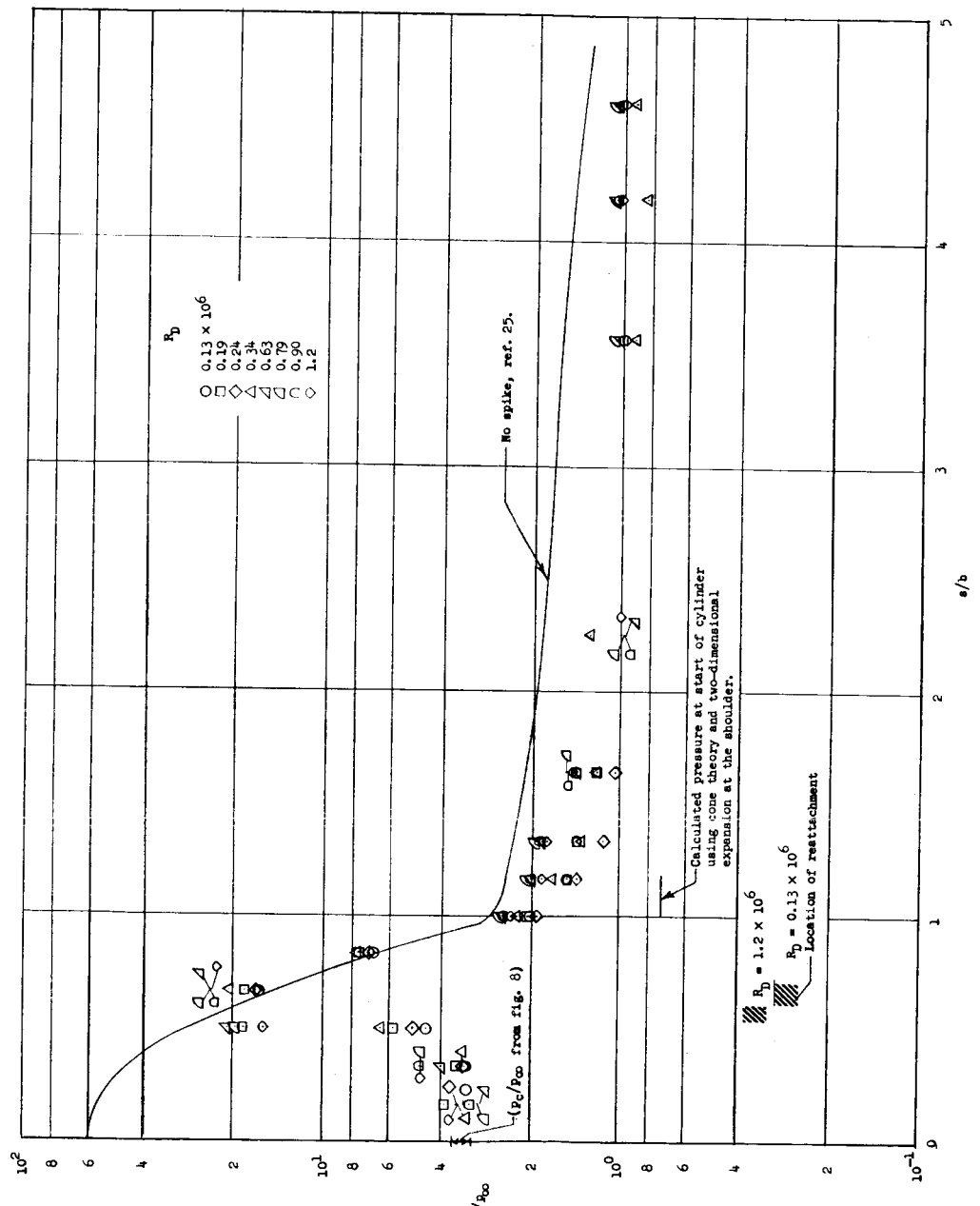


(c) L/D = 2.

Figure 12.- Continued.

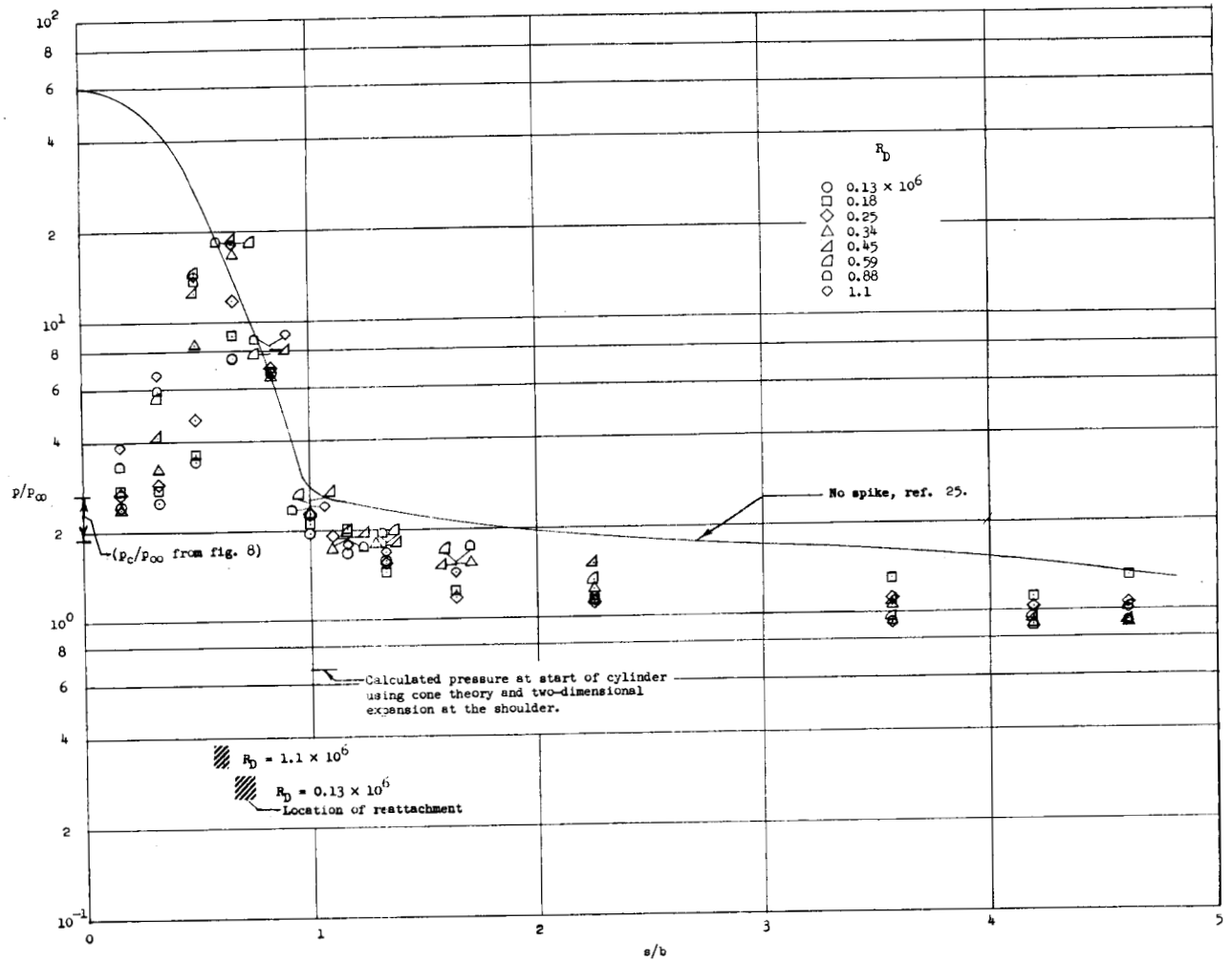


(d) L/D = 3.

Figure 12.- Continued.

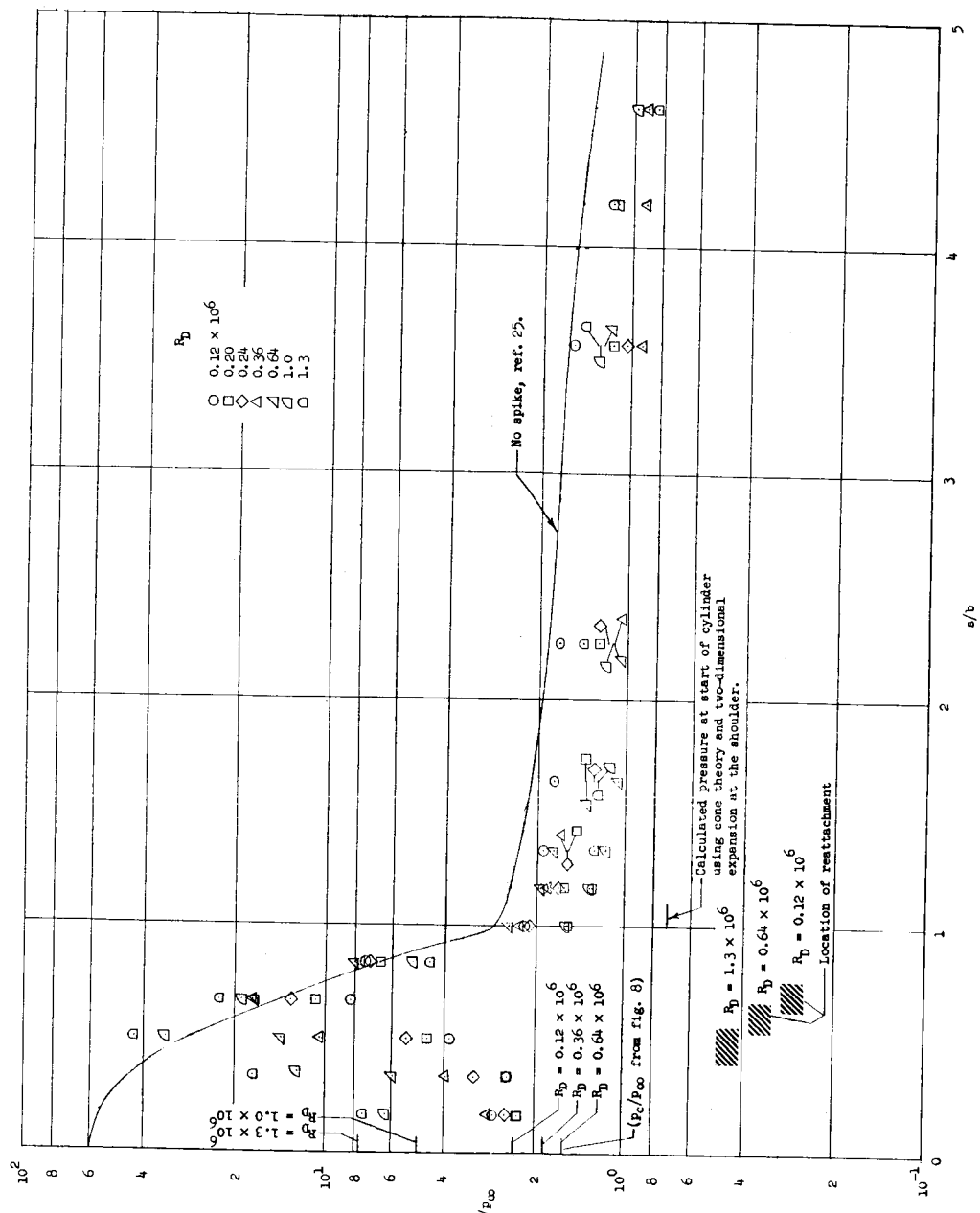


(e) L/D = 4.

Figure 12.- Concluded.

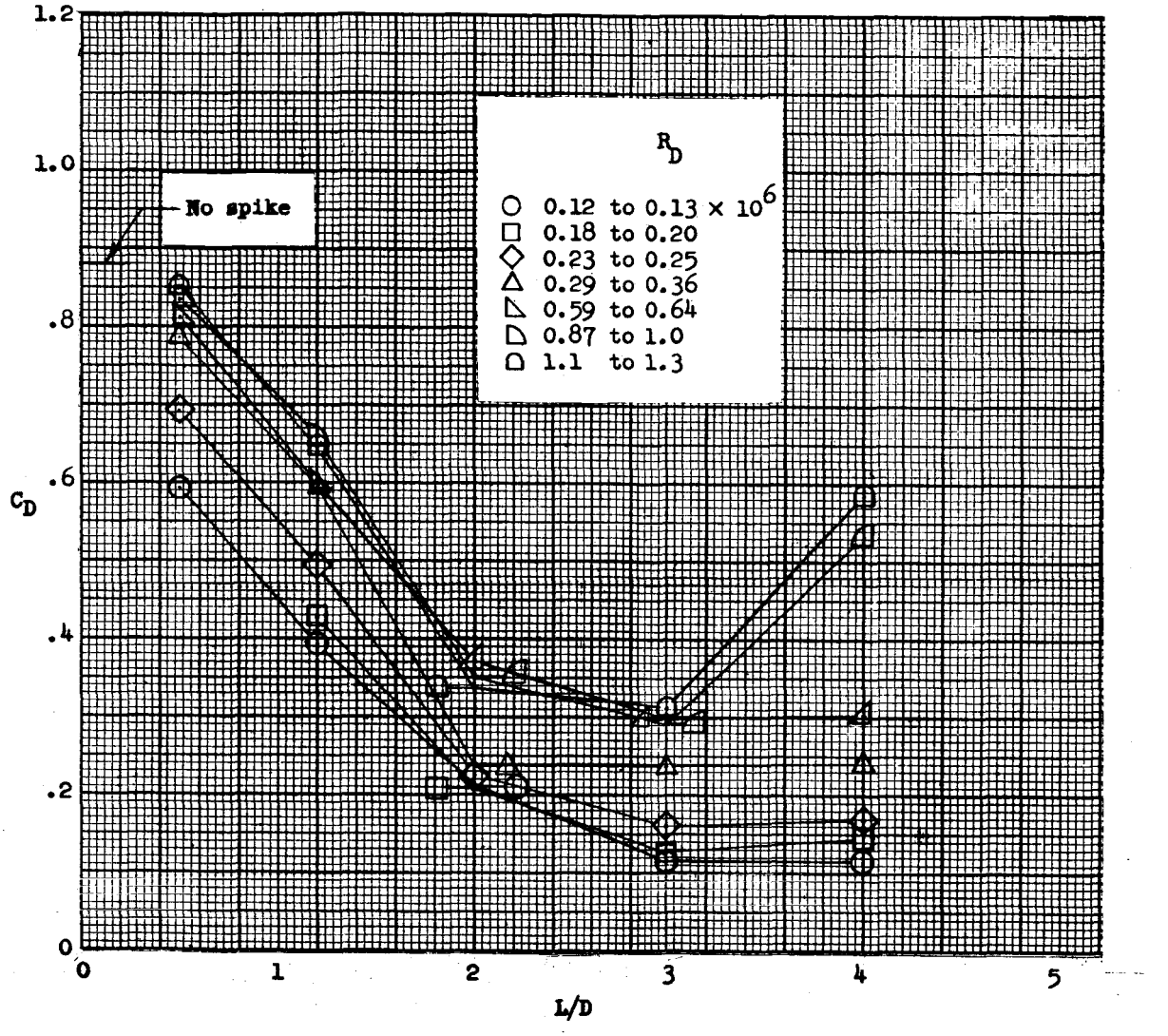


Figure 13.- Effect of spike length upon the pressure drag coefficient of the spiked-nose hemisphere.

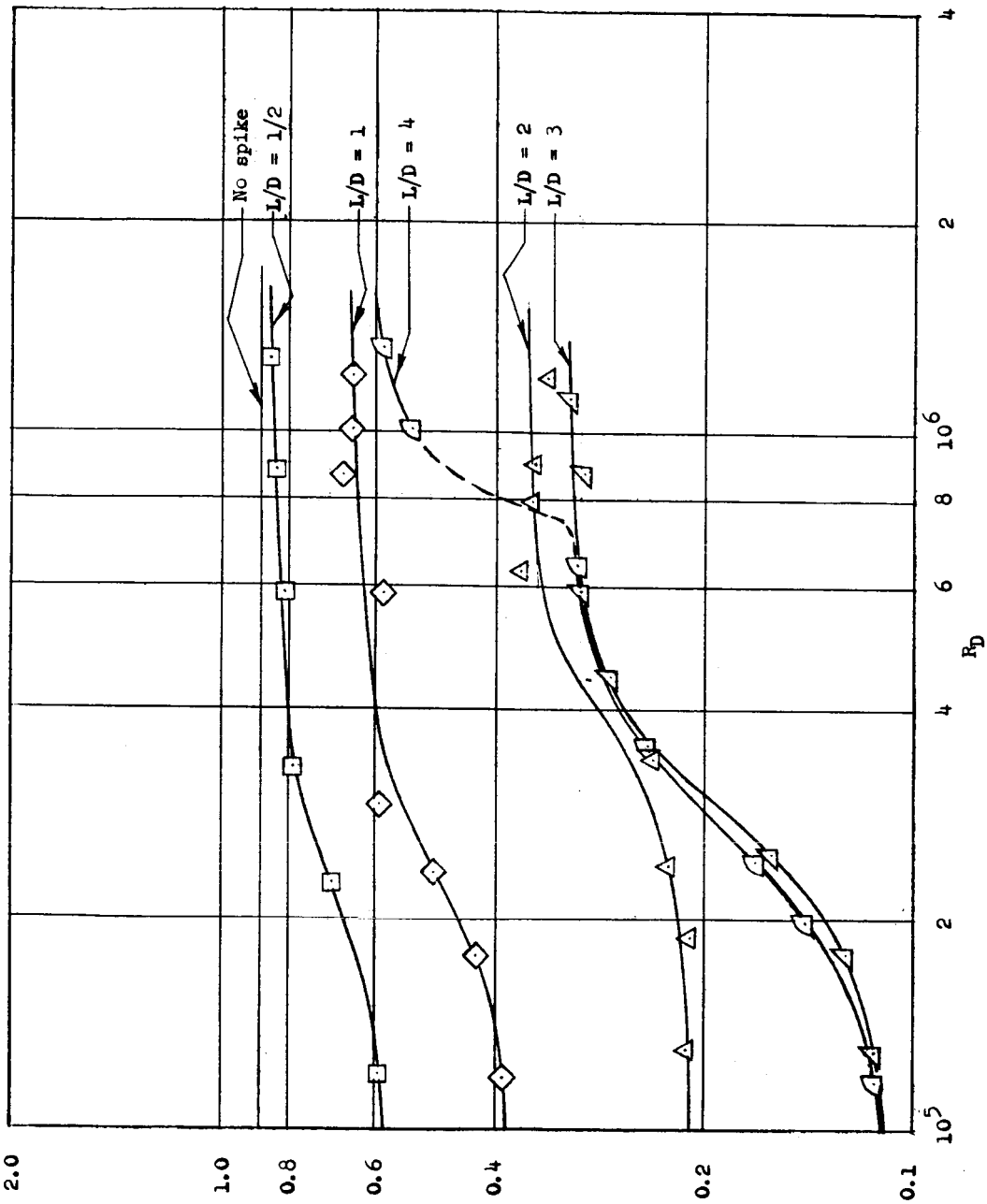


Figure 14.- Effect of Reynolds number upon the pressure drag coefficient of the spiked-nose hemisphere.

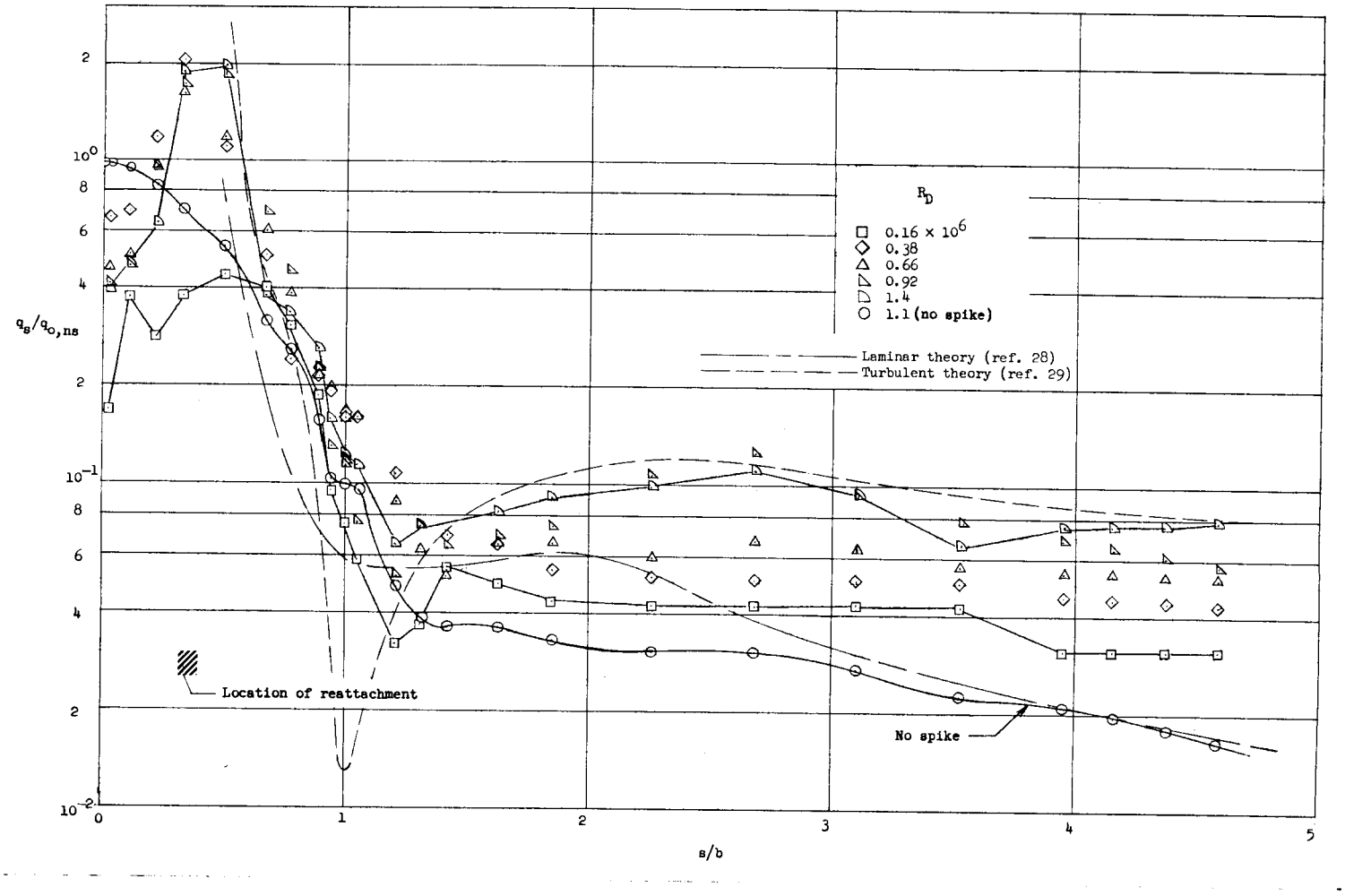


(a) L/D = 1/2.

Figure 15.- Effect of Reynolds number upon local heat transfer to spiked-nose hemisphere-cylinder.

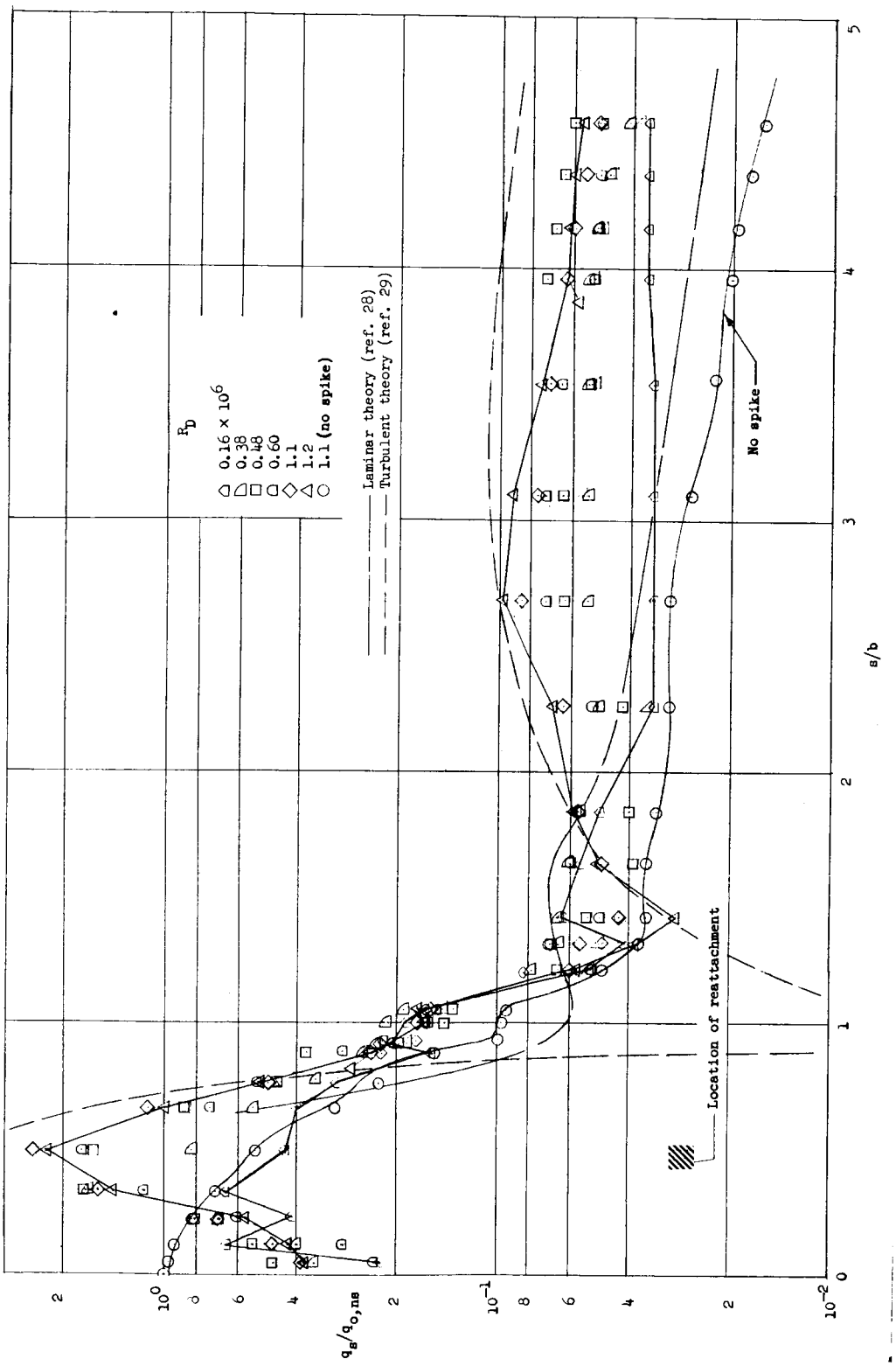


(b) L/D = 1.

Figure 15.- Continued.

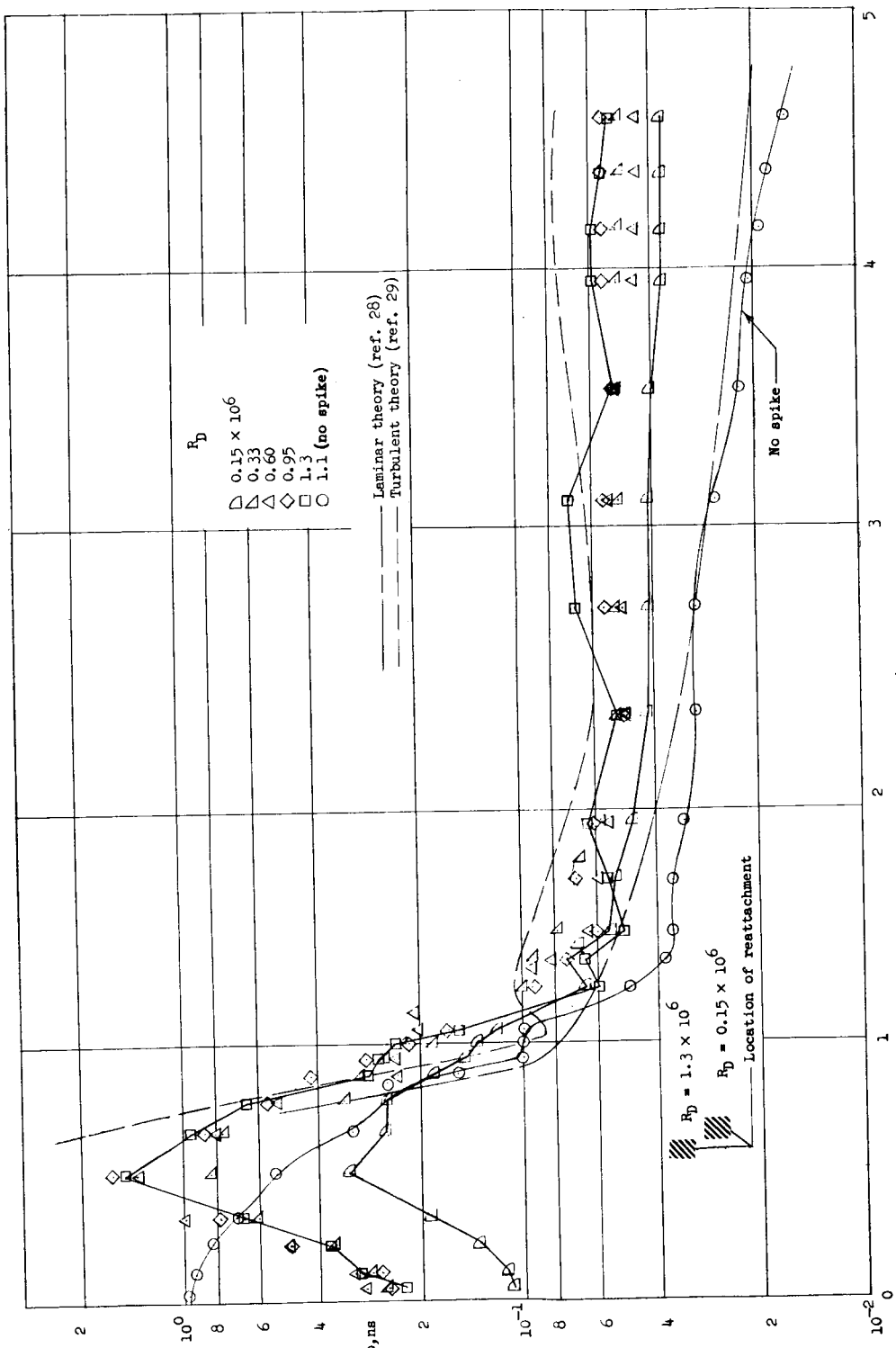


(c) L/D = 2.

Figure 15.- Continued.

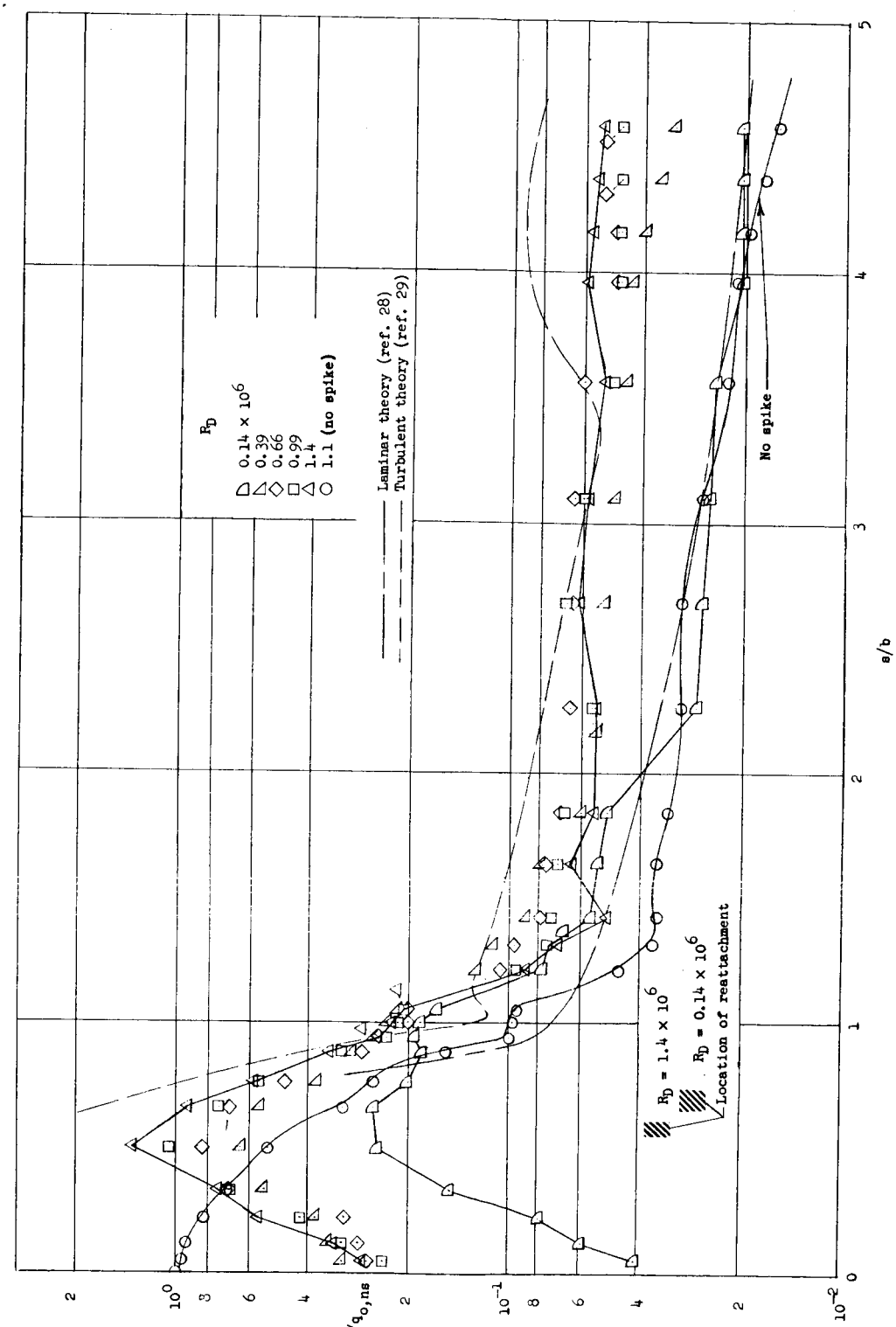


(d) L/D = 3

Figure 15.- Continued.

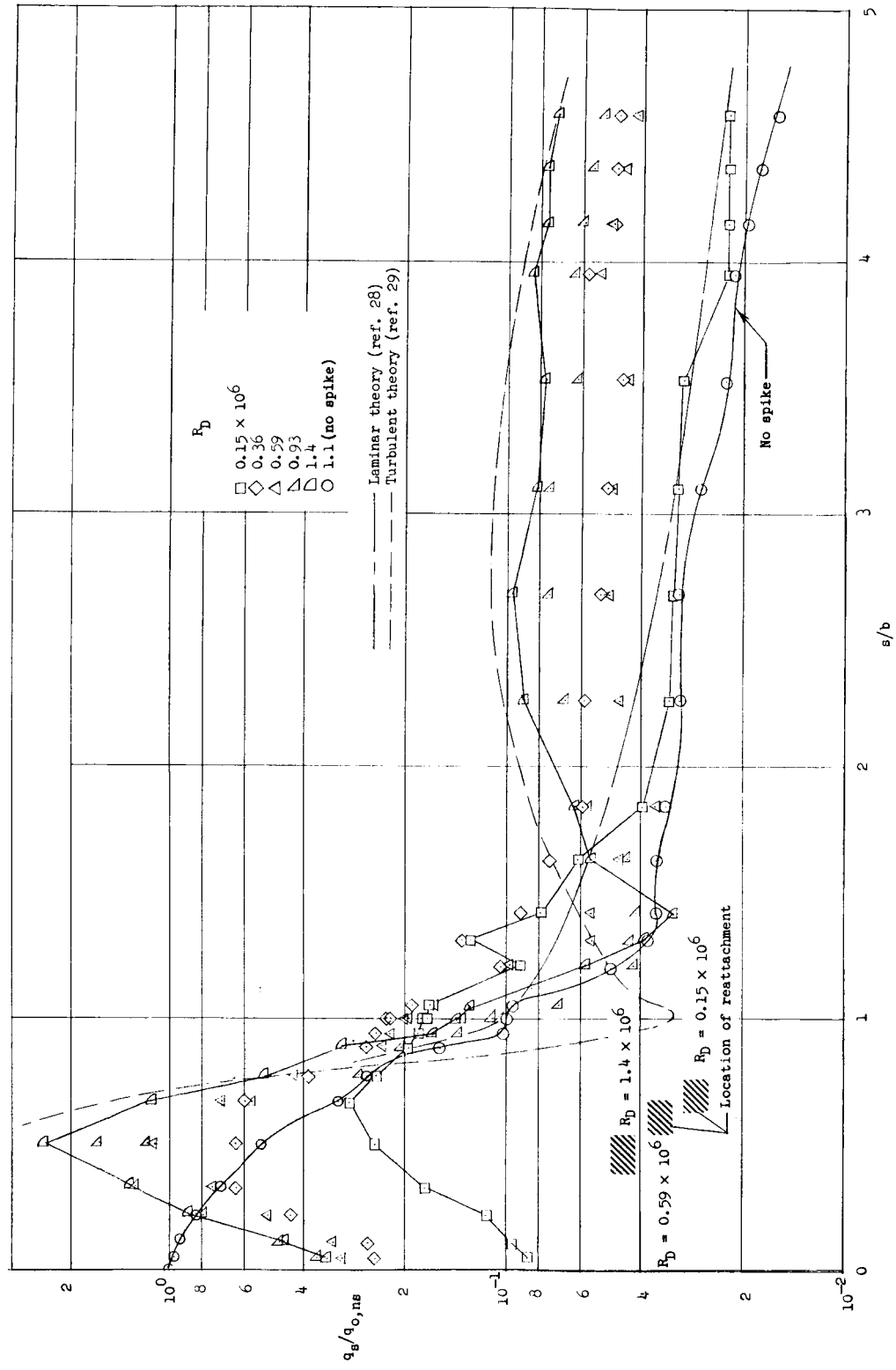


(e) L/D = 4.

Figure 15.- Concluded.

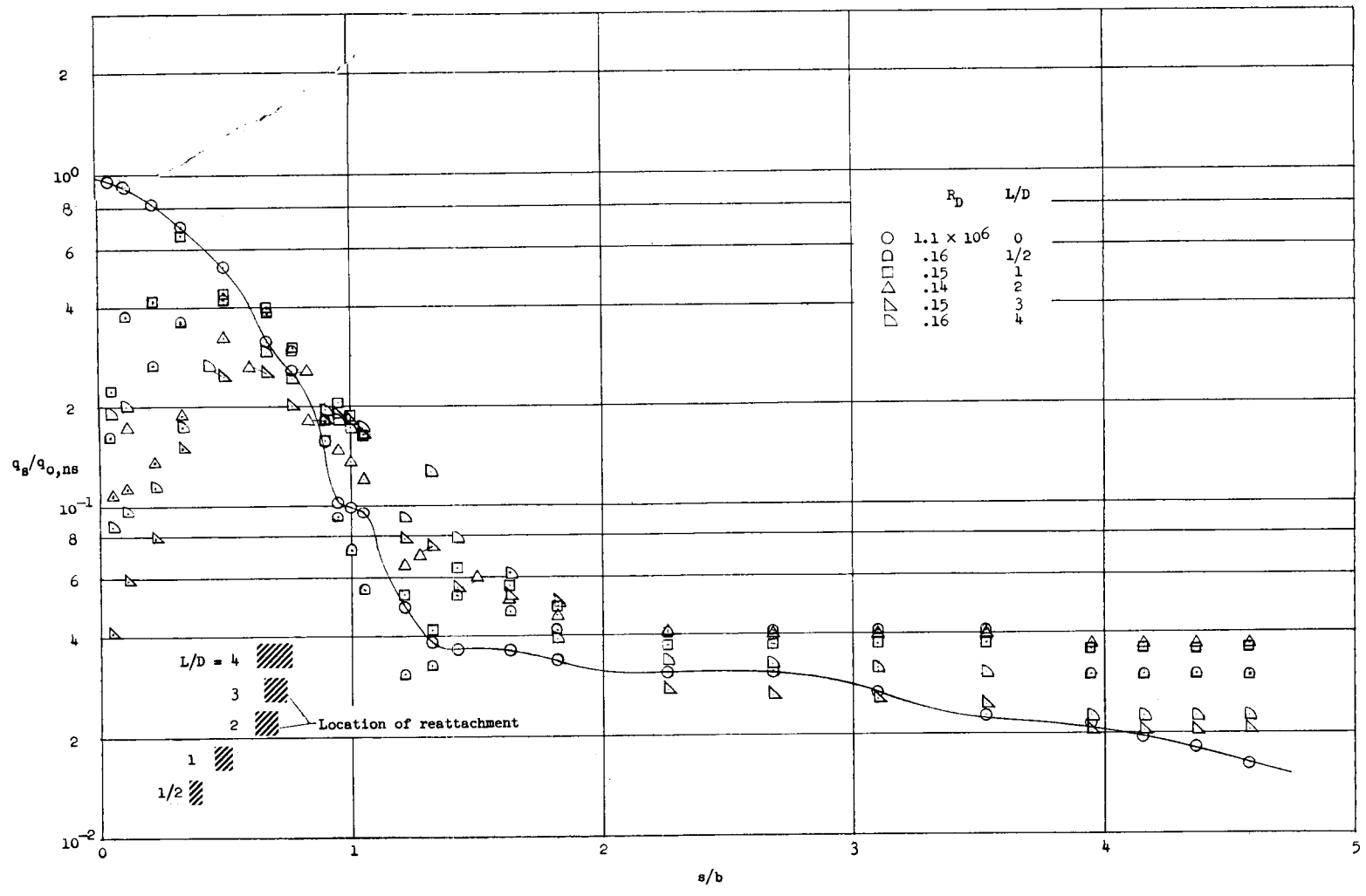


(a) $0.14 \times 10^6 \leqq R_D \leqq 0.16 \times 10^6$.

Figure 16.- Effect of spike length upon local heat transfer to spiked-nose hemisphere-cylinder.

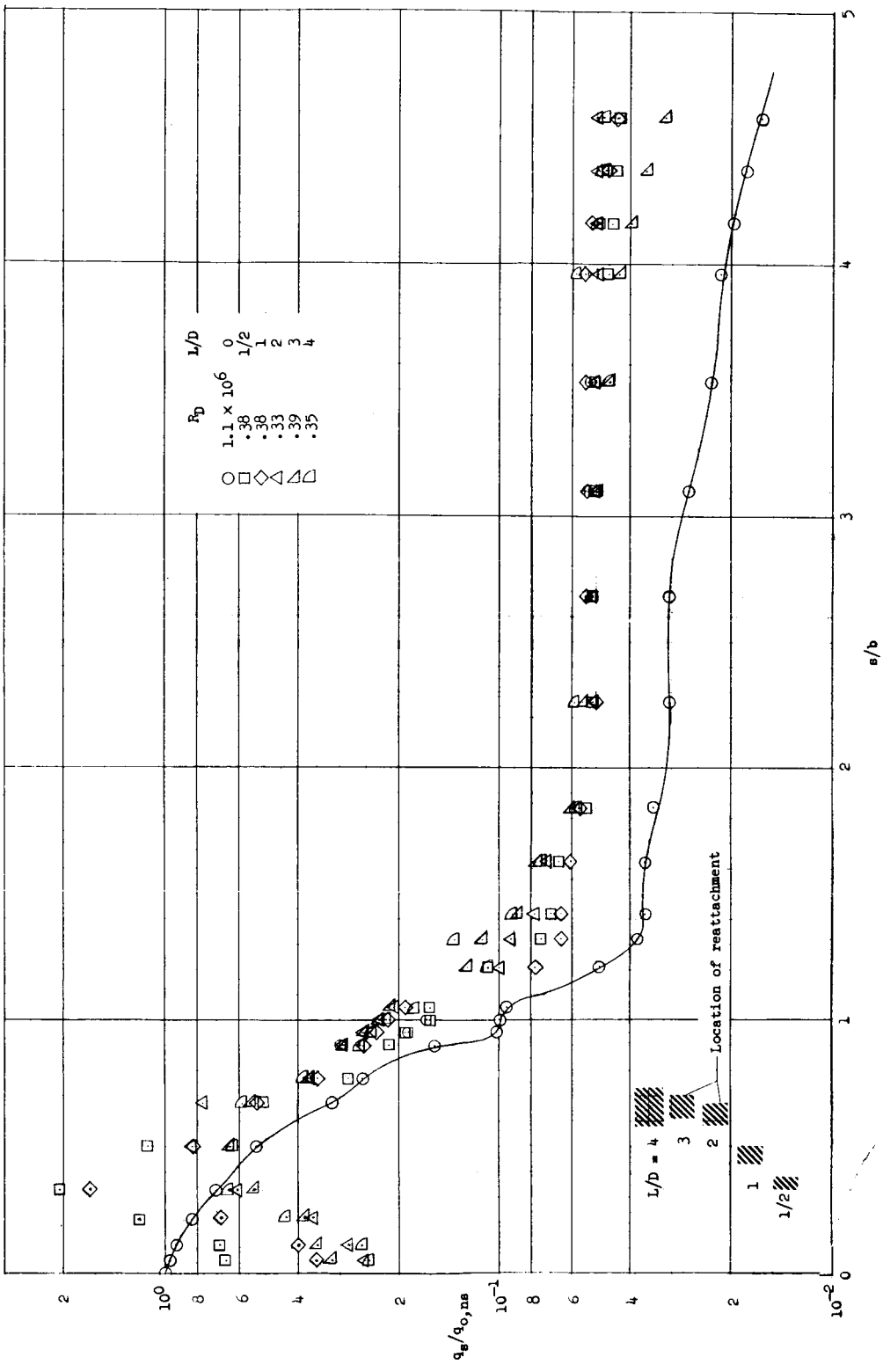


(b) $0.33 \times 10^6 \leq R_D \leq 0.39 \times 10^6$.

Figure 16.- Continued.

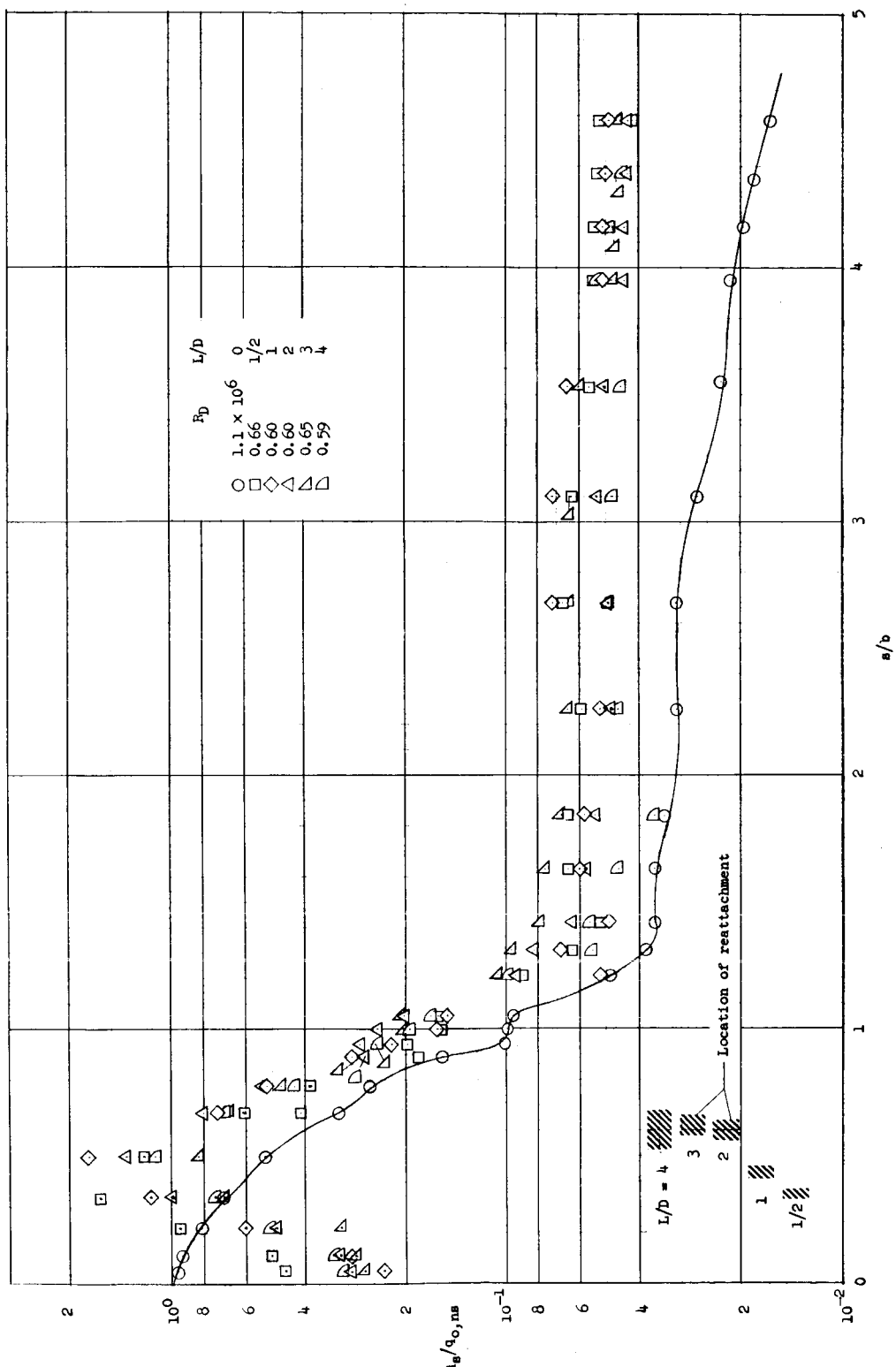


(c) $0.59 \times 10^6 \leq R_D \leq 0.66 \times 10^6$.

Figure 16.- Continued.

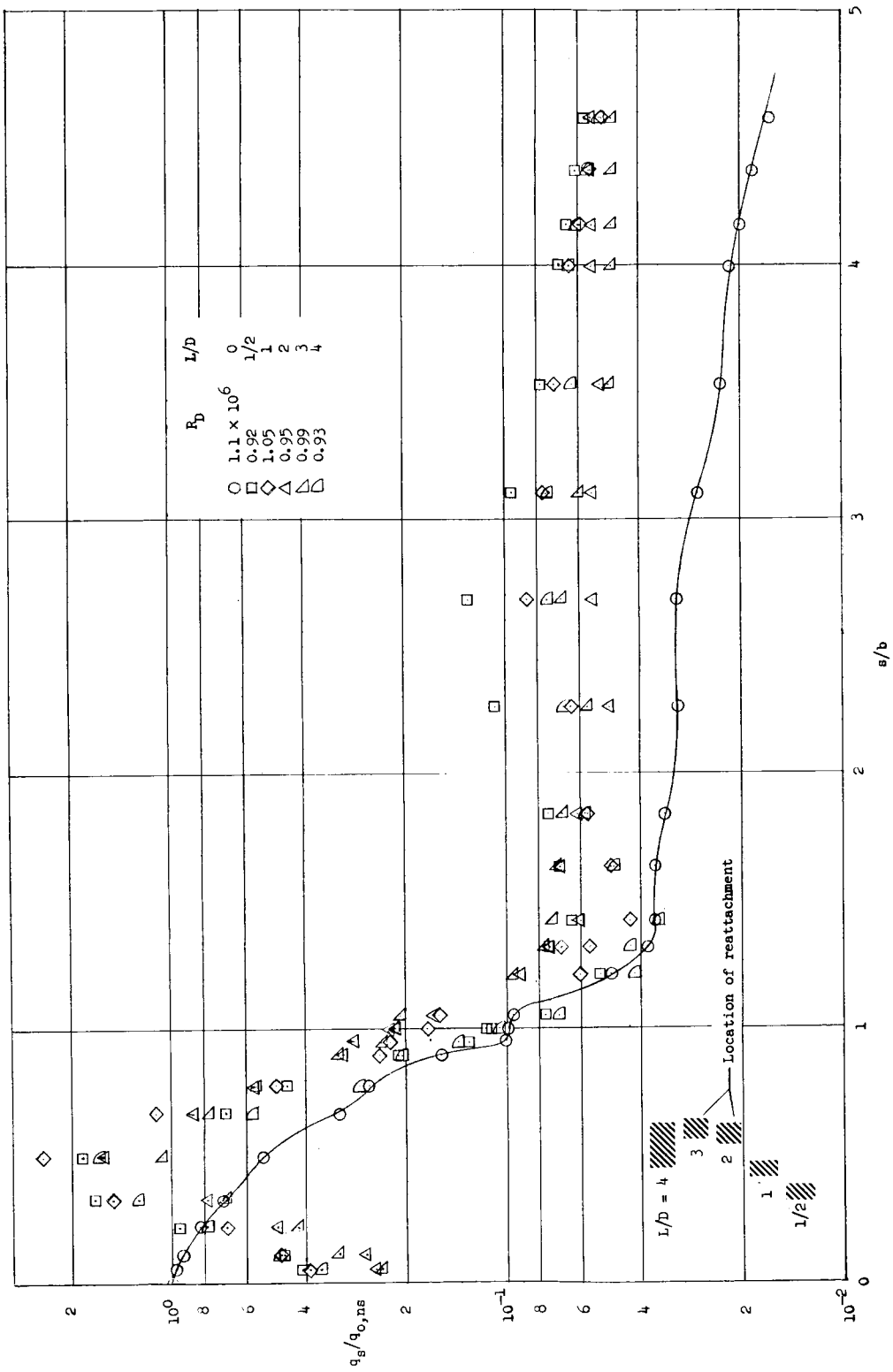


(d) $0.92 \times 10^6 \leq R_D \leq 1.05 \times 10^6$.

Figure 16.- Continued.

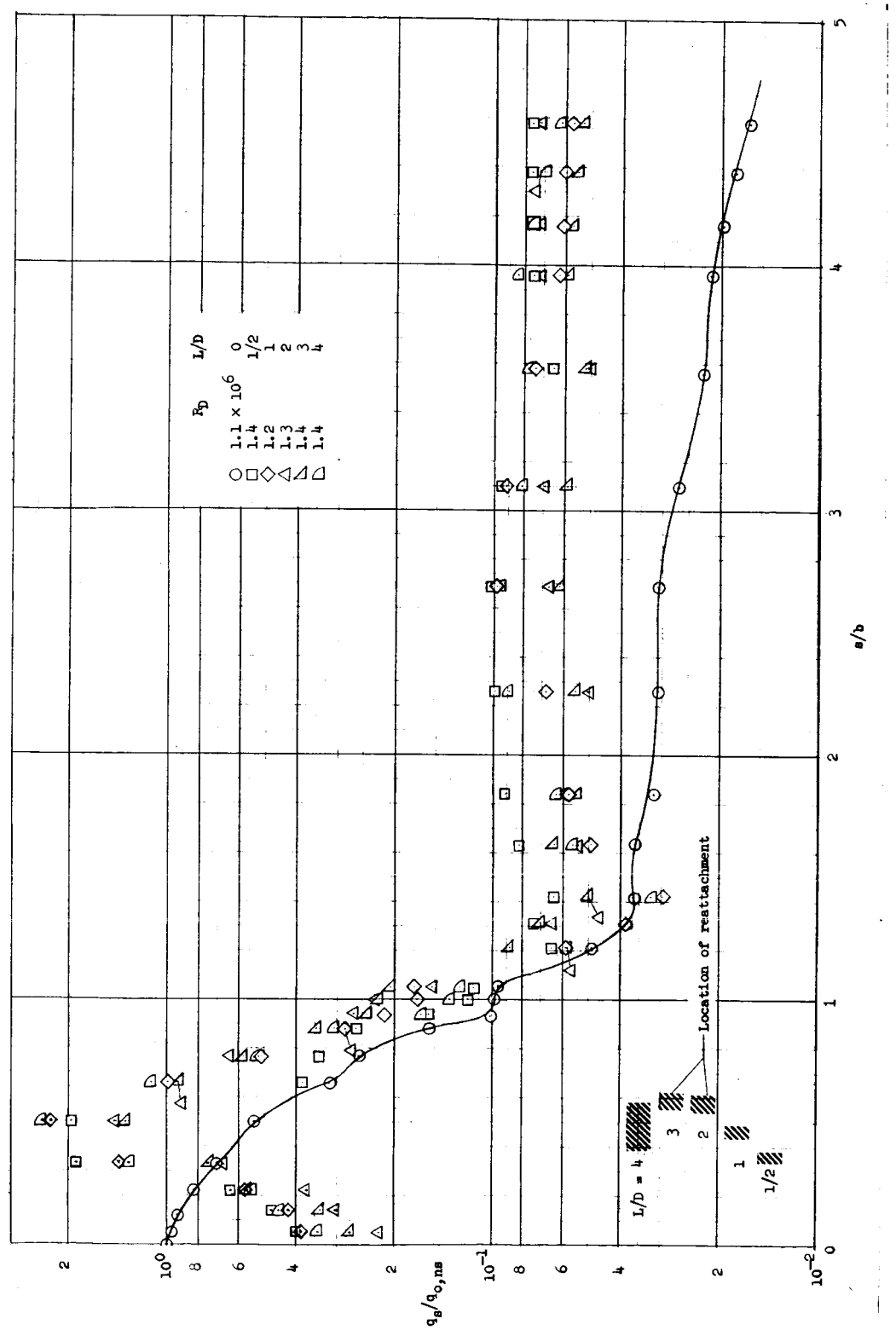


(e) $1.2 \times 10^6 \leq R_D \leq 1.4 \times 10^6$.

Figure 16.- Concluded.

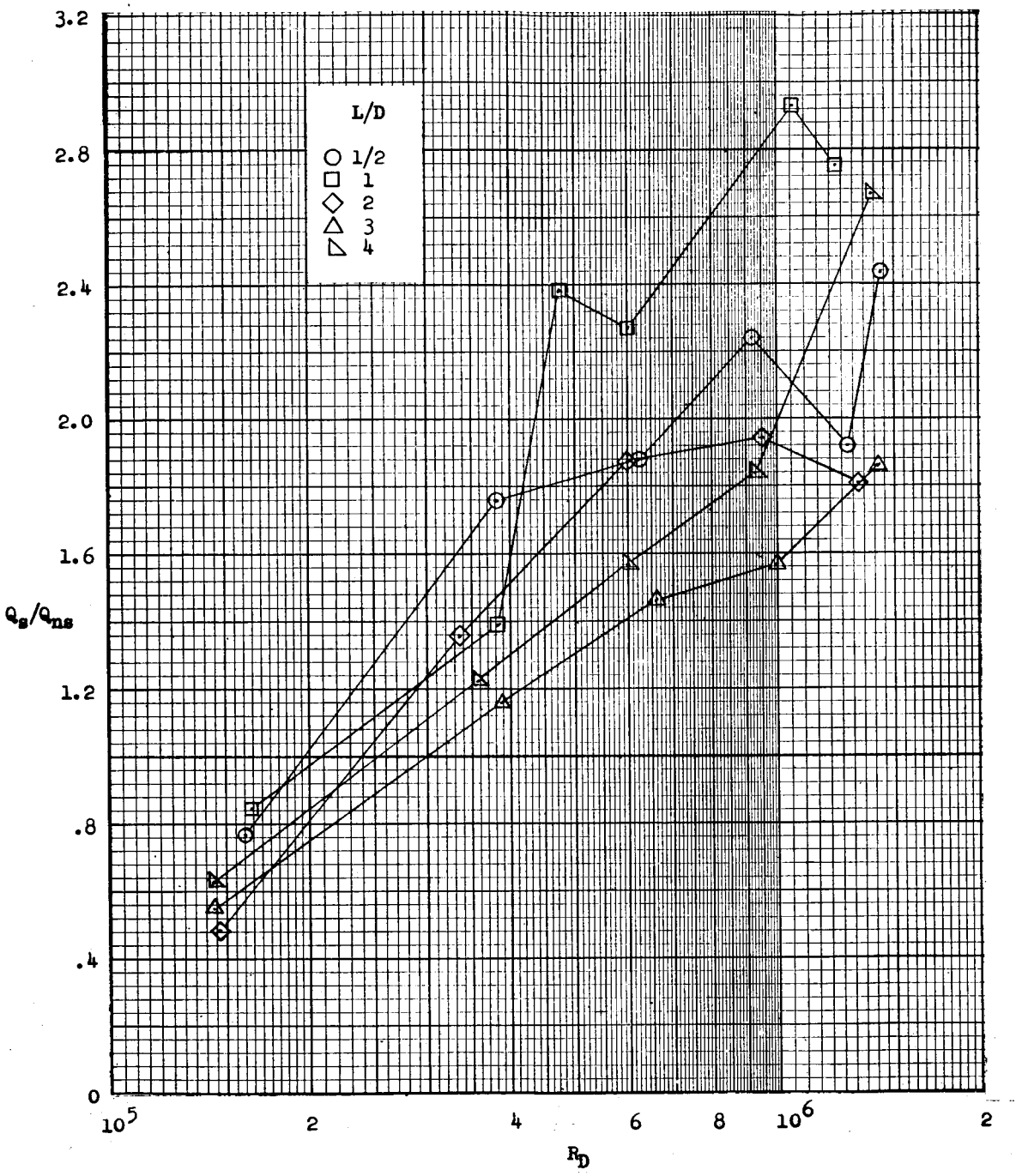


Figure 17.- Effect of spike length and Reynolds number upon integrated heat transfer to spiked-nose hemisphere-cylinder.

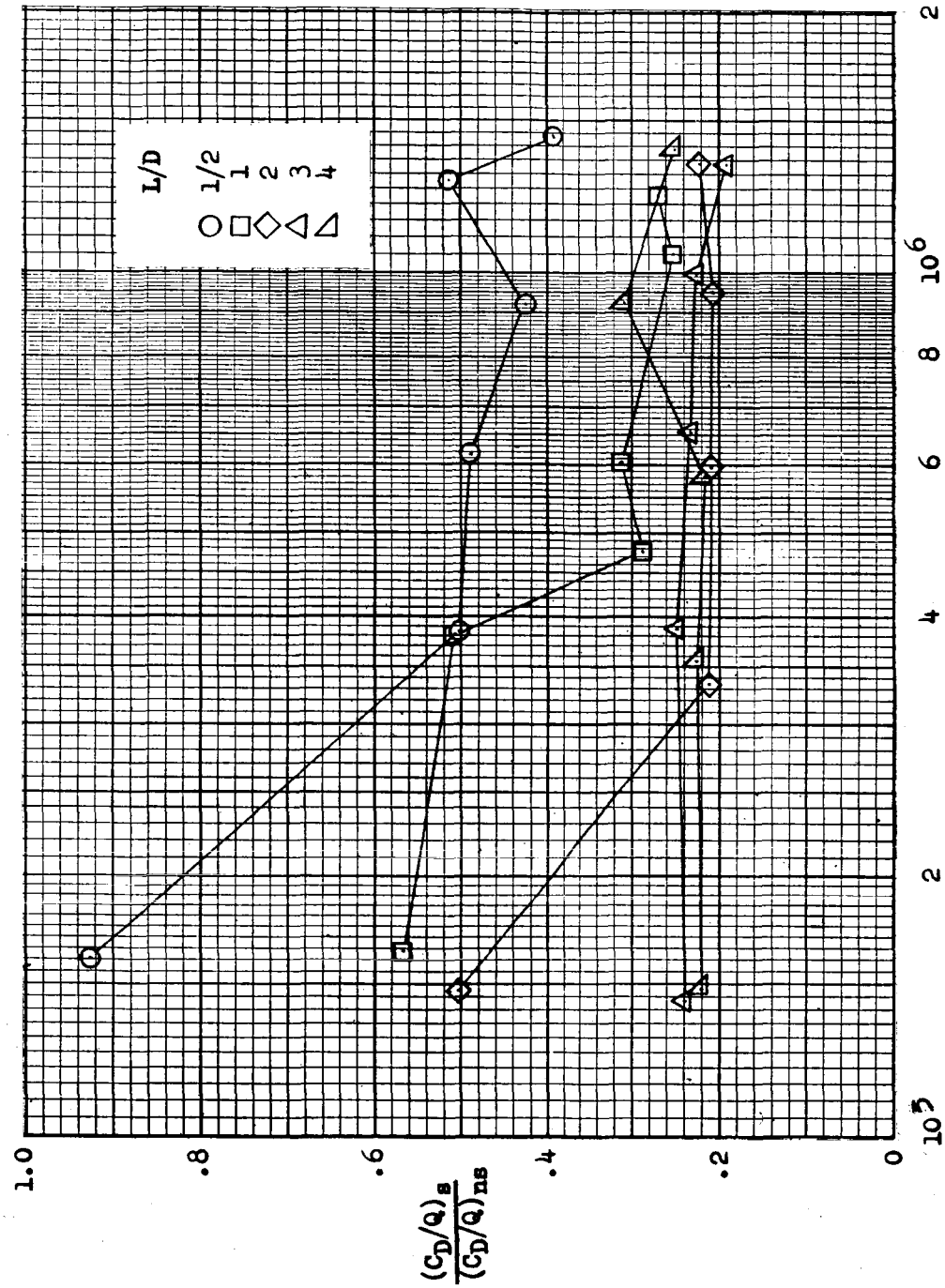


Figure 18.- Effect of Reynolds number and spike length upon the ratio of drag coefficient to total heat input to spiked hemisphere-nose.